Greenland Ice Sheet Rainfall, Heat and Albedo Feedback Impacts From the Mid-August 2021 Atmospheric River

Jason Box, Adrien Wehrlé, Dirk van As, Robert Fausto, Kristian Kjeldsen, Armin Dachauer, Andreas Ahlstrøm, Ghislain Picard

Greenland Ice Sheet Rainfall, Heat and Albedo Feedback Impacts from the Mid-August 2021 Atmospheric River

Jason E. Box[1], Adrien Wehrlé[2], Dirk van As[1], Robert S. Fausto[1], Kristian K. Kjeldsen[1], Armin Dachauer[1], Andreas P. Ahlstrøm[1], Ghislain Picard[3,1]

[1] Geological Survey of Denmark and Greenland (GEUS), Copenhagen, Denmark
[2]Institute of Geography, University of Zürich, Zürich, Switzerland
[3]UGA, CNRS, Institut des Géosciences de l'Environnement (IGE), Grenoble, France

Corresponding author: Jason Box (jeb@geus.dk)

Key Points

1. A mid-August 2021 Greenland atmospheric river produced extreme ice sheet snow cover changes and high proglacial river discharge.
2. Surface heating from rainfall is small compared to latent and sensible heating, net longwave radiation or sunlight absorption.
3. Melt-albedo feedback enhanced upper elevations snow melt under clear skies following the heating delivered by the atmospheric river.

Abstract Rainfall at the Greenland ice sheet Summit 14 August, 2021, was delivered by an atmospheric river (AR). Extreme surface ablation expanded the all-Greenland bare ice area to near-record-high with snowline climbing up to 788±90 m. Ice sheet wet snow extent reached 46%, a record high for the 15-31 August AMSR data since 2003. Heat-driven firn deflation averaged 0.14±0.05 m at four accumulation area automatic weather stations (AWSs). Energy budget calculations from AWS data indicate that surface heating from rainfall is much smaller than from either the sensible, latent, net-longwave or solar energy fluxes. Sensitivity tests show that without the heat-driven snow-darkening, melt at 1840 m would have totaled 28% less. Similarly, at 1270 m elevation, without the bare ice exposure, melting would have been 51% less. Proglacial river discharge was the highest on record since 2006 for late August and confirms the melt-sustaining effect of the albedo feedback.

Plain Language Summary While rainfall at Summit station atop of the Greenland Ice Sheet in mid-August, 2021 captured global attention, its direct surface thermal effects were weak and unable to explain the major melt and river discharge that occurred during and after the event. Exceptional heating of the ice sheet first occurred due to the heat transfer from condensation and the elevated air temperature during an atmospheric river episode. Satellite measurements reveal a rapid retreat of the snowline to higher elevations, exposing a large extent of relatively dark bare ice. Where snow remained, darkening due to wet snow metamorphism was responsible for sustained additional solar heating of the upper ice sheet elevations for the following two weeks. Observations from automatic weather stations and satellites, and river gauging, reveal that the atmospheric river had an immediate and sustained impact.

Keywords

- Greenland ice sheet
- Atmospheric River
- Albedo feedback

1. Introduction

On 14 August, 2021, news headlines reported that rainfall was witnessed for the first time at Summit station near the highest point of the Greenland ice sheet (Ramirez, 2021) and was accompanied by high surface melt extent (Scambos et al., 2021).

Greenland rainfall can be delivered as part of concentrated poleward transport of moisture and heat in “atmospheric rivers” (ARs). Neff et al. (2014) identified ARs promoting Greenland melting by movement of air masses over the ocean with upstream development over the 2012 summer North American heatwave. The 2012 ARs were responsible for the largest observed single-day Greenland surface ice ablation rate of 0.28 m day^{-1} (Fausto et al., 2016; Fausto et al., 2016; Mattingly et al., 2018). In addition to increasing Greenland rainfall fraction of precipitation (Niwano et al., 2021), the frequency of moist ARs reaching Greenland is also increasing (Mattingly et al., 2016), likely driven by more highly-amplified jet-stream patterns (Francis & Skific, 2015). ARs have strong surface energy budget impacts (Mattingly et al., 2020), yet so far lack an analysis including on-ice rainfall observations.

Atmospheric heating induces snow darkening via snow grain metamorphism (Brun, 1989; Picard et al., 2012; Wiscombe & Warren, 1980) and dark bare ice exposure (Ryan et al., 2019; Wehrlé et al., 2021). Because snow grain growth occurs as a cube

of liquid water content (Brun et al., 1992), small amounts of rain or meltwater can rapidly lower clean snow albedo with the observed cloud-free clean snow albedo range from 0.85 to 0.60 (Cuffey & Paterson, 2006). On glaciers, once snow ablates, the bare ice albedo can decline below the initial exposed bare ice albedo of 0.57±0.11 (Wehrlé et al., 2021) to below 0.25 (van As et al., 2013) mainly from ice microbiological processes (Cook et al., 2020; Ryan et al., 2018; Stibal et al., 2017; Williamson et al., 2020). Thus, the Greenland ice sheet surface mass balance can be thought of as highly responsive through melt-albedo feedback (Flanner et al., 2011; Qu & Hall, 2007).

Here, surface glacial and proglacial hydrological impacts of the mid-August, 2021 atmospheric river event are examined using automatic weather station records, satellite-derived wet snow and bare ice extents, snow and bare ice albedo, snowline elevation and proglacial meltwater river discharge data. A surface energy budget model is used to quantify radiative, turbulent, and rainfall heat transfers for melting before, during and after the atmospheric river.

2. Data and Methods

2.1. AWS Meteorological Observations

Automatic Weather Station (AWS) data from the Greenland Climate Network (GC-Net) (Steffen et al., 1996; Steffen & Box, 2001) and the Programme for the Monitoring of the Greenland ice sheet (PROMICE) (Ahlstrøm et al., 2008; Fausto et al., 2021) provide in-situ microclimatological observations. AWS albedo is computed using a running ±11-hour sum of upward/downward solar irradiance after (van den Broeke et al., 2004). New are Lufft WS401-UMB rain gauges initiated by GEUS starting June, 2021 on GC-Net stations and from 2018 on the NUK_U PROMICE

station. Rain gauge undercatch-correction and rainfall heat transfer details appear in Supporting Information.

2.2. Sentinel-3 Retrievals

Satellite retrievals of snow and ice albedo are from the EU Copernicus Sentinel-3A Ocean Land Colour Instrument (OLCI). These Snow and Ice (SICE) albedo retrievals agree within 5% with the PROMICE AWS observations (Kokhanovsky et al., 2019, 2020). Cloud identification employs Sentinel-3A Sea and Land Surface Temperature Radiometer (SLSTR) data after (Metsämäki et al., 2015). The SICE algorithms and data appear in open access repositories (Box et al., 2020; Wehrlé et al., 2020).

2.2.1. Image Analysis

To increase clear sky coverage before and after the rain and AR event, we form average albedo mosaics; 9-13 August and 15-19 August, 2021. From these, 100 m elevation-binned albedo averages are taken from three areas of interest (Figure 1b) and compared with AWS data. For estimates of average snowline position, we take the bare ice to snow albedo threshold of 0.565 after (Wehrlé et al., 2021).

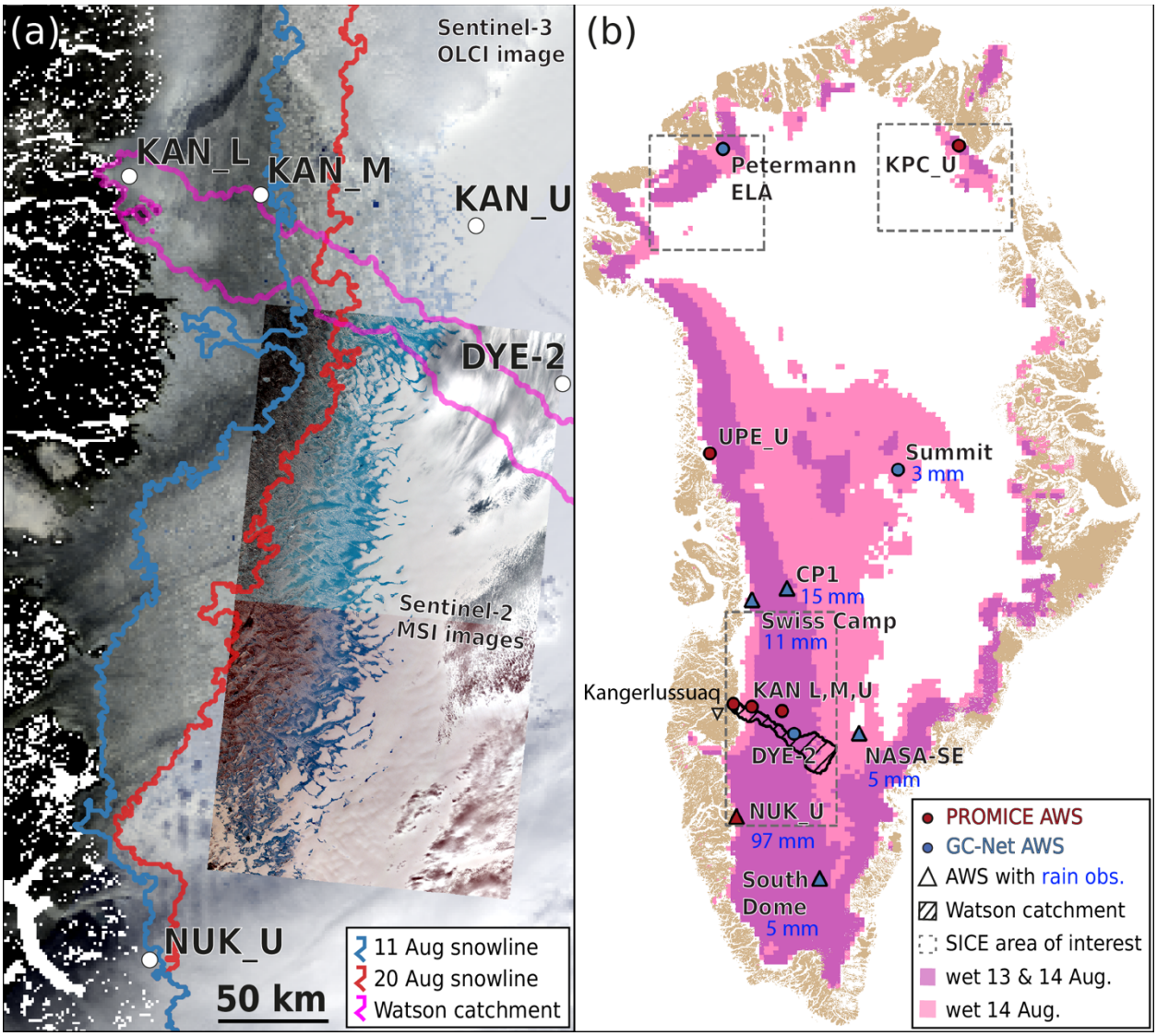

Figure 1. Automatic weather station (AWS) locations and the Watson River catchment appear on both panels. (a) An area of the western Greenland ice sheet on 20 August, 2021 featured using a 1 km Sentinel-3 OLCI RGB image with inset 10 m Sentinel-2B true color images illustrating saturated snow and dark bare ice after the atmospheric river. (b) GC-Net and PROMICE AWS locations and the expansion of wet snow area over 12-hours recorded by AMSR satellite passive microwave between August 13, 16 UTC and August 14, 04 UTC. Rain amounts at AWS are indicated and described further here and in Supporting Information.

2.3. Watson River discharge and catchment surface energy budget

The Watson River, fed by a 11,922 km^2 catchment of the western Greenland ice sheet, has discharge recorded in Kangerlussuaq (van As et al., 2018) (see Figure 1 and Figure S13). Surface energy budget (SEB) data over the catchment are obtained from PROMICE KAN L, M, and U AWS data driving a SEB model (van As et al., 2017). The model solves for the surface temperature in balance with all energy fluxes: net shortwave and longwave radiation; sensible and latent heat fluxes; subsurface heat flux and rain heat flux. Turbulent heat fluxes are calculated using near-surface gradients in temperature, wind speed and humidity. Energy budget surplus contributes to melting for cases with surface temperature reaching 0°C.

2.4. AMSR Wet Snow Mapping

AMSR-E and AMSR2 satellite 19 GHz passive microwave sensors are used to map the presence of snowpack water twice-daily (13 UTC ascending and 01 UTC descending passes) with 20 km spatial resolution after (Picard & Fily, 2006; Torinesi et al., 2003). Bare ice melting below the snowline is sometimes not captured by this algorithm and is ignored, leading to underestimates of the total ice sheet melt extent by up to 6%. The interannual frequency of wet snow is evaluated using the data span from years 2003-2021.

3. Results and Discussion

3.1. Large-scale Circulation

ERA5 850 hPa wind and water vapor fields (Copernicus Climate Change Service (C3S), 2017) (Figure S1a-c) reveal a low-pressure system west of Greenland 13

August, 2021 that drew an AR from the southwest onto the island by 14 August. By 16 August, another low had invaded which re-invigorated the southerly advection to Greenland as the AR shifted eastward. Southerly air and moisture delivery to southwest Greenland continued 17 August. By 19 August, the AR connection to Greenland had ceased and large-scale winds had reduced. On 20 August, the southerly flow was offshore from Greenland and weakened. By 21 and 22 August, northerly flow brought lower air temperatures to western Greenland with high pressure and clear sky conditions prevailing over the ice sheet. The relatively dry conditions continued through 27 August. Then, until 31 August, air temperatures continued decreasing across west Greenland with sustained northerly polar air advection, punctuating the ablation season.

3.2. Snow, Melt, then Rain

All AWS with rainfall instruments (Figure 1) recorded air temperatures (T_{air}) exceeding 0°C at least eight hours before rainfall. Prior to T_{air} > 0°C and rainfall, the AWS surface height and albedo records also indicate snowfall at several sites: CP1 (Figure S6b); Summit (Figure S5a); and NUK_U (Figure 2a, Figure S4). Consistently, Sentinel-3 SICE retrievals indicate elevated albedo 11-13 August from snowfall prior to heating conditions.

3.3. AWS Site Rainfall, Albedo and Surface Height

3.3.1. NUK_U

Rainfall at NUK_U totaling 97.0 mm over three days (76 h) commenced 14 August 04 UTC (UTC is hereafter ‘z’) and continued intermittently until 20 August 00z (Figure 2a). Four days before the atmospheric river, 0.18 m snow accumulated (07 August 23z-08 August 08z, 9h). The fresh snow had ablated prior to rainfall. The large (0.4)

albedo decline caused by the atmospheric river includes bare ice exposure by 11 August. By the onset of rainfall 14 August, albedo stabilized below 0.4. Air temperatures peaked above 5°C when the highest rates of ice ablation occurred for times when rainfall is not recorded, net shortwave was relatively high (>100 W m^{-2}) and net longwave was positive, indicative of low clouds. The NUK_U ice ablation during and after the atmospheric river totaled 0.4 m, substantial at 20% of the full 2008-2019 ablation season average.

3.3.2. South Dome

5.3 mm South Dome (SDM) rainfall was measured in three pulses during 50 h from 15 August 06z-17 August 08z. The SDM record indicates snow deflation pausing when air temperatures drop below the melting point early 15 August (Figure 2b). Rainfall at this high elevation (2893 m) location indicates the extremely high heat content of the air mass.

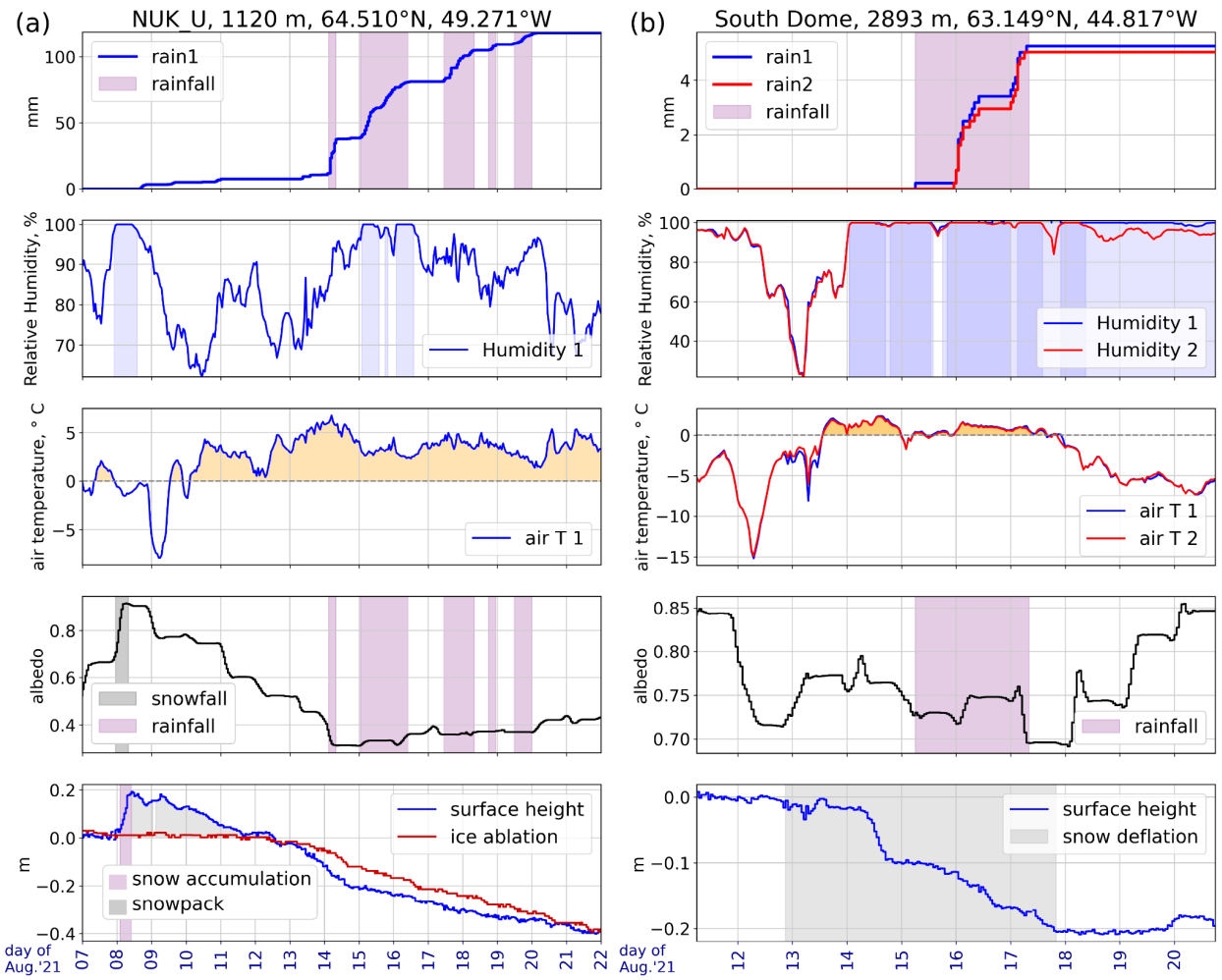

Figure 2. Rainfall, air temperature, albedo and surface height changes recorded by (a) the NUK_U PROMICE AWS (photo Figure S2) and (b) by the GEUS South Dome (SDM) GC-Net AWS photo (Figure S4). Note the differences in scale for the y-axes between sites. At SDM, instrument 1 is 1.2 m nearer the surface than instrument 2. Instrument heights start at roughly 2 m above ground. Shading is applied to the graphics to illustrate relative humidity cases above 98%, air temperature above 0°C, rainfall and snowfall cases. The NUK_U ice ablation recording is from a hydraulic sensor (Fausto et al., 2012).

3.4. Satellite Observations of Melt

At the onset of the atmospheric river 13 August, AMSR retrievals indicate a near-doubling of the ice sheet wet snow area to 9.99 x 10^5 km^2. The fractional melt area was 29% 13z 13 August, 44% by 01z 14 August, peaking at 46% at 13z on 14 August. If the bare ice area below the snow limit is included, the peak melt extent was 51%.

AMSR recorded surface melting at Summit starting at 13z on 14 August. Twelve hours earlier, no surface melting was detected in the vicinity of Summit (Figure 1b). Under the melting case at 16z, the Summit AWS (Figure S5a) recorded very low (4 W m^{-2}) solar irradiance, indicating that surface heating is likely driven by turbulent sensible and condensational heat fluxes in addition to the downward longwave irradiance.

The average number of wet snow days for the whole ice sheet for the second half of August, 2021 (4 days) was record high for the AMSR period since 2003 and twice the 2003-2021 average.

It took 8 days, until 22 August, for the wet snow extent for the whole ice sheet to return to the pre-atmospheric river extent.

3.5. Atmospheric River Impacts on Snow and Ice Albedo

The AR conditions ablated the thin snow cover across the southwestern ablation area. At NUK_U (Figure S4) and KAN_M, an extreme albedo change (-0.4) is observed as snow ablation led to dark (albedo < 0.4) bare ice exposure. Concurrently, within four days was a large (788±90 m) snowline elevation increase across the western ice sheet area of interest (Figure 3). See also Figure 1b. The darkening can include the destruction of a sun crust (Tedstone et al., 2020) and water saturation of the surface (blue areas in Figure 1, Figure S11). Above snowline

elevation, a SICE albedo drop by 0.10±0.04 (Figure 3) is equivalent in magnitude with that observed by the KAN_U and DYE-2 AWS. In Arctic snow, where the concentration of light absorbing impurities (mainly black carbon) are typically very low (under 10 ng/g) (Doherty et al., 2013; Polashenski et al., 2015). Thus, the snow heating impacts are primarily attributable to snow grain growth and the albedo decline resulting from the grain growth-driven shortwave infrared darkening (Brun, 1989; Wiscombe & Warren, 1980).

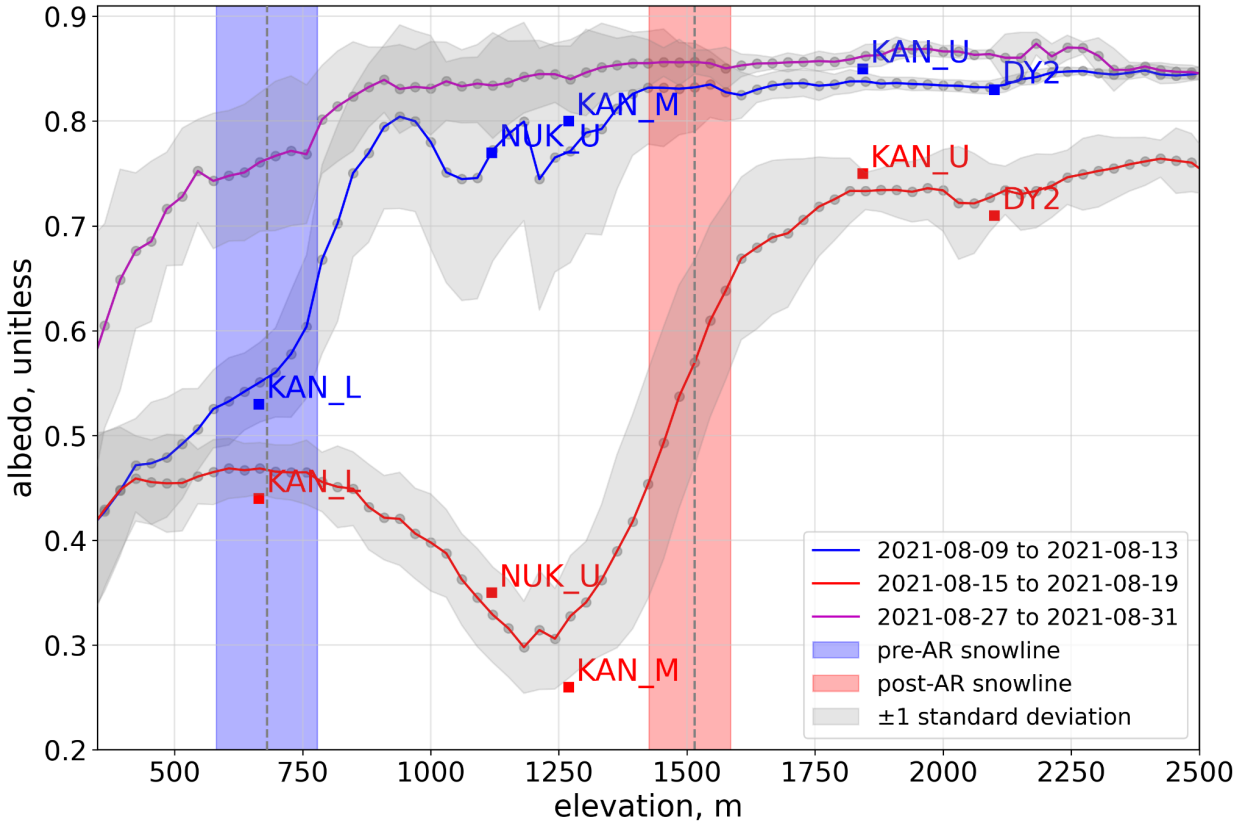

Figure 3. Averaged elevation profiles of SICE albedo including the standard deviation of the values in the specified time interval and area of interest (Fig 1b). The albedo values from field observations are included for the before and after atmospheric river (AR) cases. The color shaded areas illustrate the spreads of the snowline using ± one standard deviation from the SICE albedo and the 0.565 initial bare ice albedo after (Wehrlé et al., 2021).

The atmospheric river impacted the northern ice sheet with a snowline increase by 212±60 m on average on the Humboldt Glacier, consistent with the GC-Net Petermann AWS station recording an albedo drop of 0.16 (Figure S7). Similarly for the northeastern ice sheet, an average 121±78 m snowline increase is evident in the SICE mosaics, consistent with the 0.12 albedo drop according to the KPC_U PROMICE AWS observations (Figure S8). The SICE albedo anomaly map illustrates

widespread dark anomaly across and above much of the ice sheet ablation area, e.g. on 22 August, including the northeastern ice sheet (Figure S9), likely including foehn effects (Mattingly et al., 2020).

3.6. Surface Energy Budget

From the start of the AR, a strong increase in downward net turbulent heat transfer from the heat and moisture import initiated melt (Figure 4 red shaded area). While a stronger melt increase is observed at lower elevations (see Supporting Information and Figure S10), we feature a higher elevation site to highlight the AR impact over the much larger upper elevation accumulation area. During the AR prolongation phase (Figure 4, green area), while condensational and sensible heating and absorbed sunlight (SRNet) continue to fuel melt, key to the round-the-clock melting is the sustained positive net longwave radiation (LRNet) cf. (Charalampidis et al., 2015; Van Tricht et al., 2016).

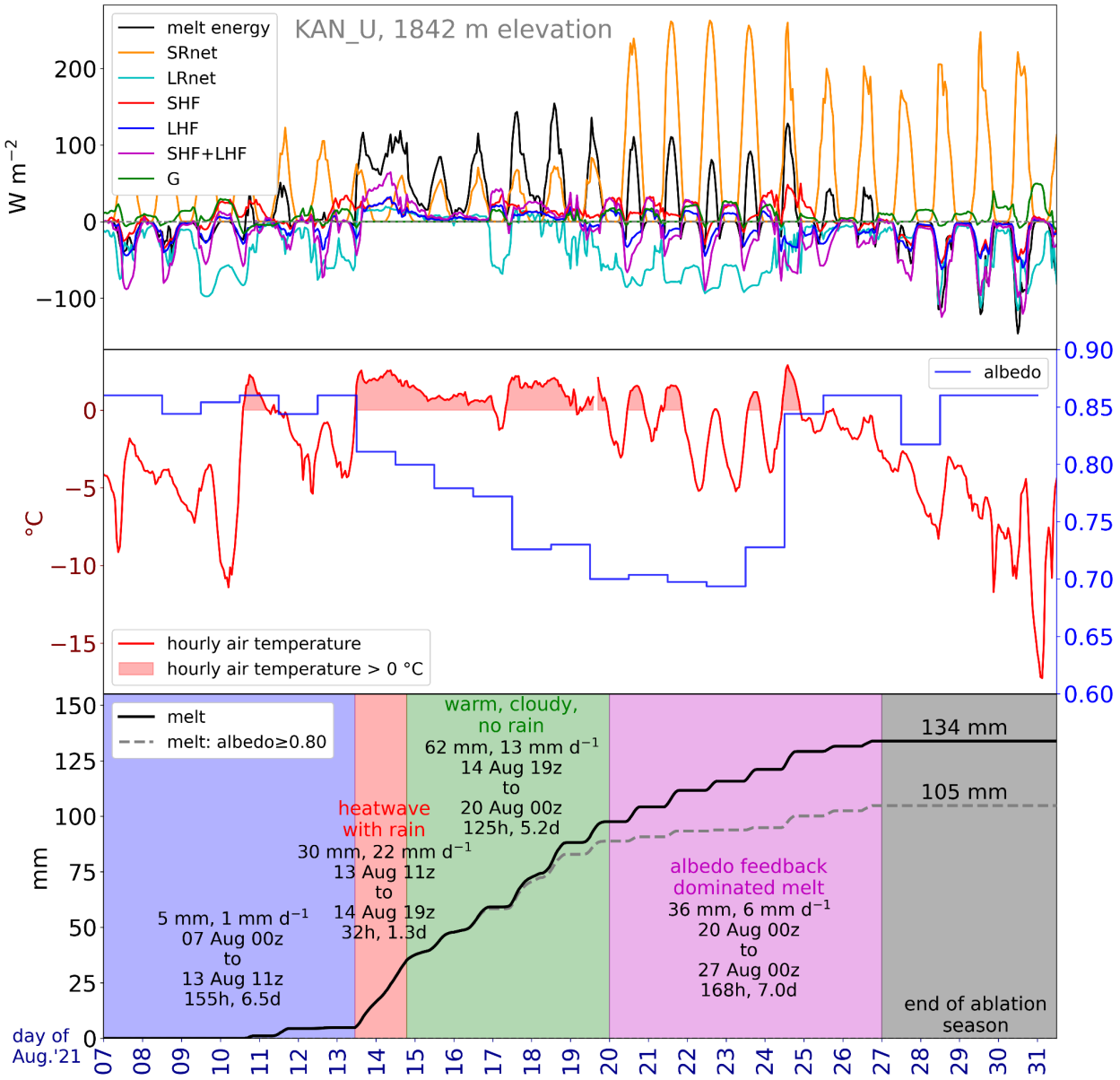

Figure 4. surface energy budget and cumulative melting at 1842 m elevation in the Watson River catchment (Figure 1) based on KAN_U AWS (See Figure S12) observations. Abbreviations: net shortwave radiation (SRNet); net longwave radiation (LRNet); sensible heat flux (SHF); latent heat flux (LHF); and ground conductive heat flux (G). The KAN sites lack rainfall observations.

Daily average air temperature at KAN_U, 1840 m above sea level, remained above melting around-the-clock 14-19 August. Subsequently, clouds began dissipating, indicated by negative trends in LRNet and turbulent fluxes (Figure 4). Yet, even as daily average T_{air} dropped below 0° C (Figure 4 purple shading), the snow albedo reduction initiated by melt during the AR and the resulting increase in SRnet sustained melting for five days (20 to 25 August). Similarly, Hofer et al. (2017) find cloud free conditions are important for the melt-albedo feedback. While some midday melting occurred, the only other surface melt energy source was a minor (<15 W m^{-2}) SHF. The cumulative melting during the melt-albedo feedback phase (Figure 4 purple area) was greater than during either the preceding AR 'heatwave' or the 'warm, cloudy, no rain' phases. Further, the rate of surface melting during the melt-albedo feedback phase was as large as the previous five days under more frequent cases of T_{air} above 0°, demonstrating the melt-albedo feedback. Were the sky conditions not mostly cloud-free, the feedback would have been less strong.

In a sensitivity calculation, by hypothetically inhibiting the snow-albedo feedback; keeping the KAN_U albedo ≥ 0.8, we found a 28% reduced melting (broken gray line on the bottom panel of Figure 4). The approximation does not include 1.) how in the brightened scenario, air temperature could drop during periods of no surface melting and 2.) that effect could not feedback into all other SEB components like the turbulent sensible heat flux or subsurface energy fluxes. Further, penetration of shortwave radiation, neglected, yields minor warming of the snow pack that may enhance melt compared to our simulations, but it is difficult to quantify without a much more complex model (van Dalum et al., 2020; Dombrovsky et al., 2019).

The end of the ablation season is accompanied by a return of high albedo (>0.8) values (Figure 4) and melt termination. See also the 27-31 August snowline elevation profile in Figure 3.

3.7. Heat from Rainfall

At CP1, while the observed total rainfall (14 mm) is 62% as large as the melt from the surface energy budget (M = 23 mm), the calculated sensible heat transfer from the CP1 rainfall amounts to just 2% the magnitude of M. Even if the rain temperature were somehow 1° C warmer, the rain contribution to surface melting would remain under 5%. Similarly, Garvelmann et al. (2014), Niwano et al. (2015) and Würzer et al. (2016) find that turbulent sensible and latent heat transfers dominate the surface energy budget, under even heavier rainfall.

The five AWS sites recording rainfall (Figure 1) indicate another limiting factor for rainfall heating of the surface. Upward longwave irradiance indicated that the surface was already melting at the onset of rainfall. Therefore, any heat-driven snow grain growth would already have begun and would not require rainfall to occur.

At Summit, a photograph of a ca. 5 mm thick ice layer is featured (Ramirez, 2021). From this and taking the refrozen layer to have had a pre-melt snow density of 300 kg m^{-3}, we estimate a rainfall of 3.4 mm, which released 1.1 MJ m^{-2} of latent energy by refreezing with rain assumed at 0°C. As the water appears to have refrozen at the surface, this released energy probably radiated away upward as decreasing air temperatures ensued after the ~8 hours of >0° C conditions. Had this water percolated to depth, the released energy would have had a considerable snow warming impact because the latent heat release (by fusion) is more than an order of magnitude higher than the specific heat of water.

3.8. Bare Ice Area

The AR surface energy budget variations in Figure 4 are evident in whole ice sheet bare ice area (BIA) changes after Wehrlé et al. (2021). The 13,337 km^2 increase in bare ice area between 19 and 20 August, 2021, right before cloudy conditions ended, was among the highest daily increase in BIA obtained by Sentinel-3 SICE retrievals in the five-year dataset (2017-2021). The BIA anomaly during the atmospheric river is 30% above the five-year average and occurs 20 days later than the previous record BIA in 2019, consistent with the results from passive microwave (See section 3.4.).

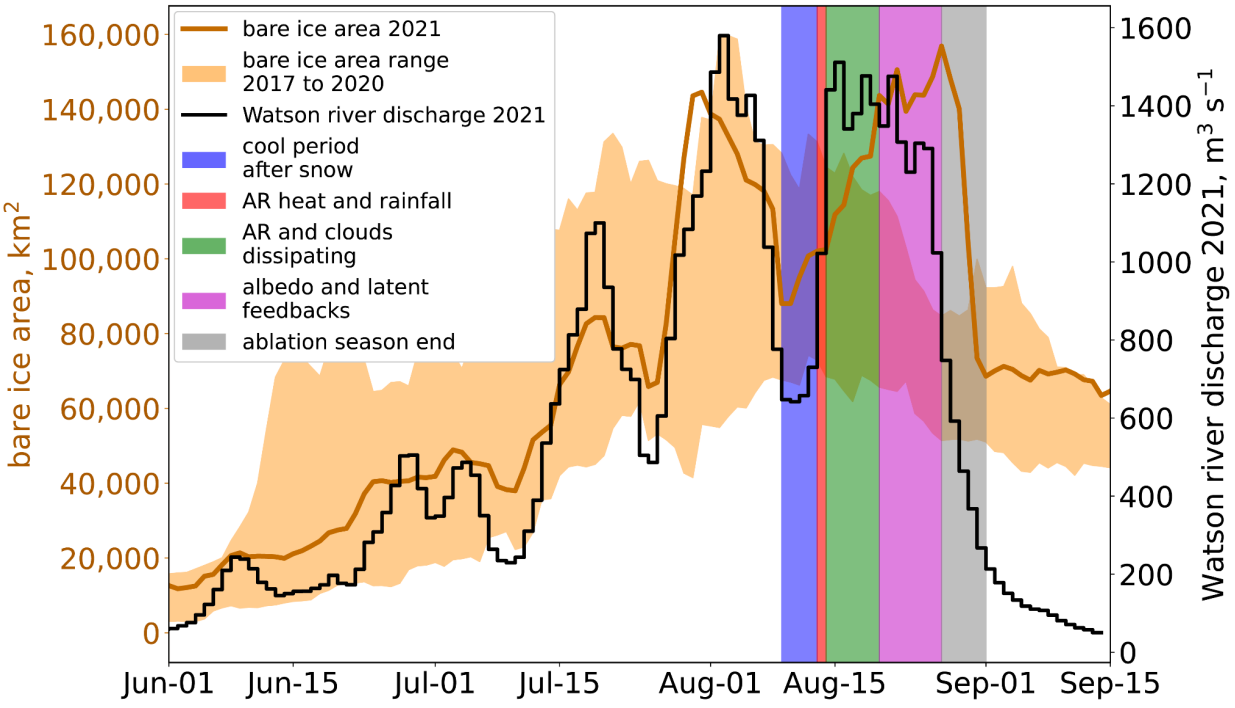

Figure 5. Greenland ice sheet bare ice area from Sentinel-3 after Wehrlé et al., (2021) and year 2021 Watson River discharge after (van As et al., 2018). Colored areas illustrate the different phases of the episode in Figure 4.

3.9. Watson River Discharge

Starting 14 August, the day of the atmospheric river, Watson River discharge increased abruptly (Figure 5). River discharge and bare ice area have a high correlation (0.858, 1-p > 0.999), suggesting the Watson River is representative of the ice sheet. The late August 2021 discharge exceeded the observed (2006-2021) annual average peak and reached above any multi-day level in the 15-27 August period of record (Figure S13). River discharge remained elevated for two weeks after the AR arrival, more than the known routing delays for the catchment (van As et al., 2017), independently demonstrating the connection of the melt-albedo feedback amplification of the AR.

4. Conclusions

The mid-August, 2021 atmospheric river (AR) produced widespread changes to snow cover extent and thickness and had strong glacio-hydrological impacts. The atmospheric river heatwave conditions were preceded by snowfall. The 2021 melt area and western river discharge was below average until the AR. However, with AR onset, a strong increase in surface turbulent sensible and latent (condensational) heat transfer to the surface drove extensive clearing of ablation area snow cover and rapid expansion of ice sheet surface melting. After clouds cleared six days later, the accumulation area snow albedo darkened by 0.1 from melt-driven wet snow metamorphism, sustaining melt conditions despite a return to sub-freezing air temperatures in early hours each day. Thus, the AR serves as a useful example of the melt-albedo feedback amplifying melt after a melt perturbation.

Satellite passive microwave data indicate how in the span of 12 hours, surface melting reached the ice sheet Summit at 04z 14 Aug, a time of day much more likely to be driven by turbulent than radiative fluxes. This single daily increase in wet snow extent for that late melt season date is the largest in the AMSR record from 2003.

The atmospheric river drove widespread snowline elevation increases; by 787±122 m for the central western ice sheet, 212±60 m for the far northwestern ice sheet (Humboldt and Petermann glaciers) and 121±78 m for the northeastern ice sheet. The loss of ablation area snow cover drove the all-Greenland bare ice area to nearly as high in the extreme melt season of 2019. The bare ice area increase, between 19 and 20 August, 2021, under cloudy conditions was among the highest daily increase in bare ice area obtained by Sentinel-3 in the first five-years of the mission.

During the AR, 0.14±0.05 m firn area snow deflation is observed by four automatic weather stations, with higher rates under non-rainy conditions, pointing to the dominance of turbulent surface heating.

Rainfall heat transfer contributed just 2% to the calculated melting at a 2200 m elevation western ice sheet site (CP1 a.k.a. Crawford Point). Condensation or sensible heat transfer from the warm air mass was a far more powerful heat source. The observed amount of melting delivered by the atmospheric river could have happened without rainfall. Yet, the impacts of rain and meltwater refreeze are considerable provided that percolation delivers the melt below where the heat can be radiated away *and* that refreeze-at-depth occurs. We found no evidence for the latter condition because the rainfall amount was not extreme and the surface was already melting hours before the rainfall. Understanding any changes to the frequency and intensity of ARs appears to be a more important research target than the heat content of the liquid precipitation atmospheric rivers may or may not produce. Further, while rainfall that does not percolate and refreeze may not have strong surface thermodynamic impacts, rainfall contribution to the hydraulics of Greenland ice (Doyle et al., 2015) may be more consequential to ablation through ice sheet flow acceleration.

The Watson River discharge for this period of August was the highest in the 16-year period of record since 2006 thus-far. The independent data from Watson River confirm the melt conditions initiated by the AR and sustained by the melt-albedo feedback. The high correlation of the river discharge with bare ice area also highlights the importance of the lower ablation area in ice sheet freshwater discharge production.

As climate warming delivers more frequent cases of the 0°C melt boundary being passed, the resilience of the ice sheet to atmospheric river heating will becomes more compromised. Had the rain instead fallen as snow, the albedo feedback would have instead been both strongly toward minimizing surface energy absorption and increasing the meltwater retention capacity. So, even while the heat added by rain is small compared to other energy sources for melt, an increasing frequency of rainfall (instead of snowfall) can have a substantial future impact on the surface mass balance and as such is a strong indication of an amplified response of the ice sheet to the effects of warming.

Without the clear-sky conditions after the AR, the albedo feedback would have been less strong. The extent of albedo-feedback-perpetuated melt may well depend on whether the cloud cover was near the surface, providing a source of perpetuated melt through surface infrared heating, as compared to a situation with high clouds which could have had a relative cooling effect.

Data Availability Statement

SICE uses open source Dataverse Project software ("Dataverse Project," 2021; King, 2007) for data curation at an open-access repository (Box et al., 2020) distributed under a non-restrictive license. Data to understand, evaluate, and build upon the reported research are available at https://doi.org/10.22008/FK2/SKBAYA

Acknowledgements

This research was funded by the European Space Agency EO Sci for Society ESRIN CCN 4000125043/18/I-NB, 2022–2023. GEUS field observations of rainfall have been supported by Greenland Integrated Observing System (GIOS), the INTAROS project under the European Union's Horizon 2020 research and innovation program under

grant agreement no. 727890 and the Danish Ministry of Climate, Energy and Utilities via The Programme for Monitoring of the Greenland Ice Sheet (PROMICE) and the Greenland Climate Network (GC-Net). AGU data policy is followed with access to related data appearing in the data availability statement. We gratefully acknowledge PROMICE and GC-Net engineers: Alan Pedersen; Jakob Jakobsen; Chris Shields, field workers: Dirk van As; Andreas Ahlstrøm; Chris Shields; Nanna Karlsson; Alan Pedersen; Derek Houtz and Øyvind Winton and WSL data scientists: Ionut Iosifescu and Rebecca Kurup. Baptiste Vandecrux is thanked for commenting on the manuscript. Stefan Hofer provided very useful constructive suggestions as an external reviewer.

CReDIT Matrix

Task	JB	AW	DVA	RSF	AD	APA	KKK	GP
Conceptualization	3	2	2	1		1		2
Data curation	2	2	1	3			1	
Formal analysis	3	3	3		1			2
Funding acquisition	1			1		2		
Investigation	3	3	1	1				1
Methodology	3	2	2					
Project administration	2			1		2		
Resources	3	1	3					2
Software	3	3	3	1	1			1
Supervision	2							1
Validation	3	2			1			
Visualization	3	2	2	1	1			
Writing	3	1	2	1	1		1	1
Writing	2	1					2	1
Sum	**36**	**22**	**19**	**10**	**5**	**5**	**4**	**11**

References

Ahlstrøm, A. P., & * PROMICE project team. (2008). A new programme for monitoring the mass loss of the Greenland ice sheet. *GEUS Bulletin*, *15*, 61–64. https://doi.org/10.34194/geusb.v15.5045

van As, D., Fausto, R. S., Colgan, W. T., Box, J. E., & * PROMICE project team. (2013). Darkening of the Greenland ice sheet due to the melt albedo feedback observed at PROMICE weather stations. *GEUS Bulletin*, *28*, 69–72. https://doi.org/10.34194/geusb.v28.4728

van As, D., Bech Mikkelsen, A., Holtegaard Nielsen, M., Box, J. E., Claesson Liljedahl, L., Lindbäck, K., et al. (2017). Hypsometric amplification and routing moderation of Greenland ice sheet meltwater release. *The Cryosphere*, *11*(3), 1371–1386. https://doi.org/10.5194/tc-11-1371-2017

van As, D., Hasholt, B., Ahlstrøm, A. P., Box, J. E., Cappelen, J., Colgan, W., et al. (2018). Reconstructing Greenland Ice Sheet meltwater discharge through the Watson River (1949–2017). *Arctic, Antarctic, and Alpine Research*. https://doi.org/10.1080/15230430.2018.1433799

Box, J. E., Mankoff, K. D., Vandecrux, B., & Wehrlé, A. (2020). SICE dataverse. *SICE Dataverse*. Retrieved from https://dataverse01.geus.dk/dataverse/sice

van den Broeke, M., van As, D., Reijmer, C., & van de Wal, R. (2004). Assessing and Improving the Quality of Unattended Radiation Observations in Antarctica. *Journal of Atmospheric and Oceanic Technology*, *21*(9), 1417–1431. https://doi.org/10.1175/1520-0426(2004)021<1417:AAITQO>2.0.CO;2

Brun, E. (1989). Investigation on Wet-Snow Metamorphism in Respect of Liquid-Water Content. *Annals of Glaciology*. https://doi.org/10.3189/s0260305500007576

Brun, E., David, P., Sudul, M., & Brunot, G. (1992). A numerical model to simulate snow-cover stratigraphy for operational avalanche forecasting. *Journal of Glaciology*, *38*(128), 13–22. https://doi.org/10.3189/S0022143000009552

Charalampidis, C., van As, D., Box, J. E., van den Broeke, M. R., Colgan, W. T., Doyle, S. H., et al. (2015). Changing surface–atmosphere energy exchange and refreezing capacity of the lower accumulation area, West Greenland. *The Cryosphere*. https://doi.org/10.5194/tc-9-2163-2015

Cook, J. M., Tedstone, A. J., Williamson, C., McCutcheon, J., Hodson, A. J., Dayal, A., et al. (2020). Glacier algae accelerate melt rates on the south-western Greenland Ice Sheet. *The Cryosphere*. https://doi.org/10.5194/tc-14-309-2020

Copernicus Climate Change Service (C3S). (2017). ERA5: Fifth generation of ECMWF atmospheric reanalyses of the global climate. Retrieved from https://cds.climate.copernicus.eu/

Cuffey, K. M., & Paterson, W. S. B. (2006). *The Physics of Glaciers*. Elsevier.

van Dalum, C. T., van de Berg, W. J., Lhermitte, S., & van den Broeke, M. R. (2020). Evaluation of a new snow albedo scheme for the Greenland ice sheet in the Regional Atmospheric Climate Model (RACMO2). *The Cryosphere*, *14*(11), 3645–3662. https://doi.org/10.5194/tc-14-3645-2020

Dataverse Project. (2021). Retrieved 2021, from https://dataverse.org/

Doherty, S. J., Grenfell, T. C., Forsström, S., Hegg, D. L., Brandt, R. E., & Warren, S. G. (2013).

Observed vertical redistribution of black carbon and other insoluble light-absorbing particles in melting snow. *Journal of Geophysical Research*, *118*, 5553–5569. https://doi.org/10.1002/jgrd.50235

Dombrovsky, L. A., Kokhanovsky, A. A., & Randrianalisoa, J. H. (2019). On snowpack heating by solar radiation: A computational model. *Journal of Quantitative Spectroscopy & Radiative Transfer*, *227*, 72–85. https://doi.org/10.1016/j.jqsrt.2019.02.004

Doyle, S. H., Hubbard, A., van de Wal, R. S. W., Box, J. E., van As, D., Scharrer, K., et al. (2015). Amplified melt and flow of the Greenland ice sheet driven by late-summer cyclonic rainfall. Nature Geoscience, 8(8), 647–653. https://doi.org/10.1038/ngeo2482.

Fausto, R. S., Van As, D., Ahlstrøm, A. P., & Citterio, M. (2012). Assessing the accuracy of Greenland ice sheet ice ablation measurements by pressure transducer. *Journal of Glaciology*. https://doi.org/10.3189/2012jog12j075

Fausto, R. S., van As, D., Box, J. E., Colgan, W., & Langen, P. L. (2016). Quantifying the Surface Energy Fluxes in South Greenland during the 2012 High Melt Episodes Using In-situ Observations. *Frontiers in Earth Science*, *4*. https://doi.org/10.3389/feart.2016.00082

Fausto, R. S., As, D., Box, J. E., Colgan, W., Langen, P. L., & Mottram, R. H. (2016). The implication of nonradiative energy fluxes dominating Greenland ice sheet exceptional ablation area surface melt in 2012. *Geophysical Research Letters*. https://doi.org/10.1002/2016gl067720

Fausto, R. S., van As, D., Mankoff, K. D., Vandecrux, B., Citterio, M., Ahlstrøm, A. P., et al. (2021). Programme for Monitoring of the Greenland Ice Sheet (PROMICE) automatic weather station data. *Earth System Science Data*, *13*(8), 3819–3845.

https://doi.org/10.5194/essd-13-3819-2021

Flanner, M. G., Shell, K. M., Barlage, M., Perovich, D. K., & Tschudi, M. A. (2011). Radiative forcing and albedo feedback from the Northern Hemisphere cryosphere between 1979 and 2008. *Nature Geoscience*, *4*(3), 151–155. https://doi.org/10.1038/ngeo1062

Francis, J., & Skific, N. (2015). Evidence linking rapid Arctic warming to mid-latitude weather patterns. *Philosophical Transactions. Series A, Mathematical, Physical, and Engineering Sciences*, *373*(2045). https://doi.org/10.1098/rsta.2014.0170

Førland, E. J., Norske Meteorologiske Institutt., & Nordic Working Group on Precipitation (NWGP). (1996). Manual for operational correction of Nordic precipitation data. Oslo: Norwegian Meteorological Institute. Retrieved from https://www.worldcat.org/title/manual-for-operational-correction-of-nordic-precipitation-data/oclc/473734066

Garvelmann, J., Pohl, S., & Weiler, M. (2014). Variability of Observed Energy Fluxes during Rain-on-Snow and Clear Sky Snowmelt in a Midlatitude Mountain Environment. *Journal of Hydrometeorology*, *15*(3), 1220–1237. https://doi.org/10.1175/JHM-D-13-0187.1

Hofer, S., Tedstone, A. J., Fettweis, X., & Bamber, J. L. (2017). Decreasing cloud cover drives the recent mass loss on the Greenland Ice Sheet. *Science Advances*, *3*(6), e1700584. https://doi.org/10.1126/sciadv.1700584

King, G. (2007). An Introduction to the Dataverse Network as an Infrastructure for Data Sharing. *Sociological Methods & Research*, *36*(2), 173–199. https://doi.org/10.1177/0049124107306660

Kokhanovsky, A., Lamare, M., Danne, O., Brockmann, C., Dumont, M., Picard, G., et al. (2019). Retrieval of Snow Properties from the Sentinel-3 Ocean and Land Colour

Instrument. *Remote Sensing*, *11*(19), 2280. https://doi.org/10.3390/rs11192280

Kokhanovsky, A., Box, J. E., Vandecrux, B., Mankoff, K. D., Lamare, M., Smirnov, A., & Kern, M. (2020). The Determination of Snow Albedo from Satellite Measurements Using Fast Atmospheric Correction Technique. *Remote Sensing*, *12*(2), 234. https://doi.org/10.3390/rs12020234

Mattingly, K. S., Ramseyer, C. A., Rosen, J. J., Mote, T. L., & Muthyala, R. (2016). Increasing water vapor transport to the Greenland Ice Sheet revealed using self-organizing maps: INCREASING GREENLAND MOISTURE TRANSPORT. *Geophysical Research Letters*, *43*(17), 9250–9258. https://doi.org/10.1002/2016gl070424

Mattingly, K. S., Mote, T. L., & Fettweis, X. (2018). Atmospheric river impacts on Greenland ice sheet surface mass balance. *Journal of Geophysical Research*, *123*(16), 8538–8560. https://doi.org/10.1029/2018jd028714

Mattingly, K. S., Mote, T. L., Fettweis, X., van As, D., Van Tricht, K., Lhermitte, S., et al. (2020). Strong Summer Atmospheric Rivers Trigger Greenland Ice Sheet Melt through Spatially Varying Surface Energy Balance and Cloud Regimes. *Journal of Climate*, *33*(16), 6809–6832. https://doi.org/10.1175/JCLI-D-19-0835.1

Metsämäki, S., Pulliainen, J., Salminen, M., Luojus, K., Wiesmann, A., Solberg, R., et al. (2015). Introduction to GlobSnow Snow Extent products with considerations for accuracy assessment. *Remote Sensing of Environment*, *156*, 96. https://doi.org/10.1016/j.rse.2014.09.018

Neff, W., Compo, G. P., Martin Ralph, F., & Shupe, M. D. (2014). Continental heat anomalies and the extreme melting of the Greenland ice surface in 2012 and 1889. *Journal of*

Geophysical Research: Atmospheres. https://doi.org/10.1002/2014jd021470

Niwano, M., Aoki, T., Matoba, S., Yamaguchi, S., Tanikawa, T., Kuchiki, K., & Motoyama, H. (2015). Numerical simulation of extreme snowmelt observed at the SIGMA-A site, northwest Greenland, during summer 2012. The Cryosphere. https://doi.org/10.5194/tc-9-971-2015

Niwano, M., Box, J. E., Wehrlé, W., Vandecrux, B., Colgan, W. T., & Cappelen, J. (2021). Rainfall on the Greenland ice sheet: present-day climatology from a high-resolution non-hydrostatic polar regional climate model. Geophysical Research Letters.Picard, G., & Fily, M. (2006). Surface melting observations in Antarctica by microwave radiometers: Correcting 26-year time series from changes in acquisition hours. *Remote Sensing of the Environment*, *104*(3), 325–336. https://doi.org/10.1016/j.rse.2006.05.010

Picard, G., Domine, F., Krinner, G., Arnaud, L., & Lefebvre, E. (2012). Inhibition of the positive snow-albedo feedback by precipitation in interior Antarctica. *Nature Climate Change*, *2*(11), 795–798. https://doi.org/10.1038/nclimate1590

Polashenski, C. M., Dibb, J. E., Flanner, M. G., Chen, J. Y., Courville, Z. R., Lai, A. M., et al. (2015). Neither dust nor black carbon causing apparent albedo decline in Greenland's dry snow zone: Implications for MODIS C5 surface reflectance. *Geophysical Research Letters*, *42*, 9319–9327. https://doi.org/10.1002/2015GL065912

Qu, X., & Hall, A. (2007). What Controls the Strength of Snow-Albedo Feedback? *Journal of Climate*, *20*(15), 3971–3981. https://doi.org/10.1175/JCLI4186.1

Ramirez, R. (2021, August 19). Rain fell at the normally snowy summit of Greenland for the first time on record. *CNN*. Retrieved from

https://edition.cnn.com/2021/08/19/weather/greenland-summit-rain-climate-change/index.html

Ryan, J. C., Hubbard, A., Stibal, M., Irvine-Fynn, T. D., Cook, J., Smith, L. C., et al. (2018). Dark zone of the Greenland Ice Sheet controlled by distributed biologically-active impurities. *Nature Communications*, *9*(1), 1065. https://doi.org/10.1038/s41467-018-03353-2

Ryan, J. C., Smith, L. C., van As, D., Cooley, S. W., Cooper, M. G., Pitcher, L. H., & Hubbard, A. (2019). Greenland Ice Sheet surface melt amplified by snowline migration and bare ice exposure. *Science Advances*, *5*(3), eaav3738. https://doi.org/10.1126/sciadv.aav3738

Scambos, T., Stroeve, J., Koenig, L., Box, J. E., & X. Fettweis, T. M. (2021). Rain at the summit of Greenland. Retrieved from http://nsidc.org/greenland-today/2021/08/rain-at-the-summit-of-greenland/

Steffen, K., & Box, J. (2001). Surface climatology of the Greenland Ice Sheet: Greenland Climate Network 1995-1999. *Journal of Geophysical Research*, *106*(D24), 33951–33964. https://doi.org/10.1029/2001jd900161

Steffen, K., Box, J. E., & Abdalati, W. (1996). *Greenland Climate Network: GC-Net* (No. 96-27). (S. C. Colbeck, Ed.). CRREL.

Stibal, M., Box, J. E., Cameron, K. A., Langen, P. L., Yallop, M. L., Mottram, R. H., et al. (2017). Algae Drive Enhanced Darkening of Bare Ice on the Greenland Ice Sheet. *Geophysical Research Letters*, *44*(22), 11,463–11,471. https://doi.org/10.1002/2017GL075958

Tedstone, A. J., Cook, J. M., Williamson, C. J., Hofer, S., McCutcheon, J., Irvine-Fynn, T., et al. (2020). Algal growth and weathering crust state drive variability in western Greenland Ice Sheet ice albedo. *The Cryosphere*, *14*(2), 521–538. https://doi.org/10.5194/tc-14-521-2020

Torinesi, O., Fily, M., & Genthon, C. (2003). Variability and Trends of the Summer Melt Period of Antarctic Ice Margins since 1980 from Microwave Sensors. *Journal of Climate*, *16*(7), 1047–1060. https://doi.org/10.1175/1520-0442(2003)016<1047:VATOTS>2.0.CO;2

Van Tricht, K., Lhermitte, S., Lenaerts, J. T. M., Gorodetskaya, I. V., L'Ecuyer, T. S., Noël, B., et al. (2016). Clouds enhance Greenland ice sheet meltwater runoff. *Nature Communications*, *7*(1), 1–9. https://doi.org/10.1038/ncomms10266

Wehrlé, A., Mankoff, K. D., Vandecrux, B., & Box, J. E. (2020). SICE Toolchain. *Snow and Ice (SICE) Snow Optical and Microphysical Retrievals from Sentinel-3*. Retrieved from https://github.com/GEUS-SICE/SICE

Wehrlé, A., Box, J. E., Niwano, M., Anesio, A. M., & Fausto, R. S. (2021). Greenland bare-ice albedo from PROMICE automatic weather station measurements and Sentinel-3 satellite observations. *GEUS Bulletin*, *47*. https://doi.org/10.34194/geusb.v47.5284

Williamson, C. J., Cook, J., Tedstone, A., Yallop, M., McCutcheon, J., Poniecka, E., et al. (2020). Algal photophysiology drives darkening and melt of the Greenland Ice Sheet. *Proceedings of the National Academy of Sciences of the United States of America*, *117*(11), 5694–5705. https://doi.org/10.1073/pnas.1918412117

Wiscombe, W. J., & Warren, S. G. (1980). A Model for the Spectral Albedo of Snow. I: Pure Snow. *Journal of the Atmospheric Sciences*. https://doi.org/10.1175/1520-0469(1980)037<2712:amftsa>2.0.co;2

Würzer, S., Jonas, T., Wever, N., & Lehning, M. (2016). Influence of Initial Snowpack Properties on Runoff Formation during Rain-on-Snow Events. *Journal of Hydrometeorology*, *17*(6), 1801–1815. https://doi.org/10.1175/JHM-D-15-0181.1

Supporting References

Førland, E. J., Norske Meteorologiske Institutt., & Nordic Working Group on Precipitation (NWGP). (1996). Manual for operational correction of Nordic precipitation data. Oslo: Norwegian Meteorological Institute. Retrieved from https://www.worldcat.org/title/manual-for-operational-correction-of-nordic-precipitation-data/oclc/473734066

Goodison, B. E., Louie, P. Y. T., & Yang, D. (1998). Solid Precipitation Measurement Intercomparison (No. 872). WMO.

Li, X., & Kopp, R. (2019). Wetbulb calculation. Retrieved from https://github.com/smartlixx/WetBulb

Sevruk, B., Ondrás, M., & Chvíla, B. (2009). The WMO precipitation measurement intercomparisons. Atmospheric Research, 92(3), 376–380. https://doi.org/10.1016/j.atmosres.2009.01.016

Yang, D., Ishida, S., Goodison, B. E., & Gunther, T. (1999). Bias correction of daily precipitation measurements for Greenland. Journal of Geophysical Research: Atmospheres. https://doi.org/10.1029/1998jd200110

Geophysical Research Letters

Supporting Information for

Greenland Ice Sheet Rainfall, Heat and Albedo Feedback Impacts from the Mid-August 2021 Atmospheric River

Jason E. Box[1], Adrien Wehrlé[2], Dirk van As[1], Robert S. Fausto[1], Kristian K. Kjeldsen[1], Armin Dachauer[1], Andreas P. Ahlstrøm[1], Ghislain Picard[3,1]

[1]Geological Survey of Denmark and Greenland (GEUS), Copenhagen, Denmark

[2]Institute of Geography, University of Zurich, Zurich, Switzerland

[3]UGA, CNRS, Institut des Géosciences de l'Environnement (IGE), Grenoble, France

Contents of this file

Text S1: Rainfall Gauge Corrections

Precipitation gauge undercatch errors and correction efforts are widely documented, e.g.(Førland et al., 1996; Goodison et al., 1998; Sevruk et al., 2009). Undercatch results from distortion of the windfield around the rain gauge (Sevruk et al., 1991) and 'wetting loss' from water droplet sticking and evaporation without the mass flux registered. The deployed Lufft WS401-UMB tipping-bucket gauges ("Lufft," 2021) may accumulate snow and thus can lead to errors from delayed melt of snow accumulated within the gauges. Here, we only consider rainfall cases when air temperatures exceed 0 °C. We apply a catch efficiency (*k*) correction for an unshielded Hellmann-type precipitation gauge under rainfall conditions after (Yang et al., 1999):

$$k = 100/(100-4.37U+0.35U^2)$$

with wind speed (U) m s^{-1} at gauge height from the AWS observations. The correction does not exceed +16% and could incur residual trace undercatch from wetting loss.

Text S2: Heat from Rain

Rain temperature, assumed to be equivalent with the wet-bulb air temperature (T_W) (Anderson et al., 1998) calculated using the AWS hourly humidity and air temperature data (Li & Kopp, 2019). We estimate the sensible heat energy flux from rainfall (RHF) as:

$$RHF = \rho_{water}\, c_P\, \Delta T\, R$$

where ρ_{water} is the water density (1000 kg m^{-3}), c_P is the specific heat of water (4,186 J kg^{-1}), ΔT is the rain to surface temperature difference (T_{rain}-$T_{surface}$) where the surface is taken to already be at melting (Kelvins), R is the rainfall rate (kg s^{-1}). The

mm water equivalent ablation rate is computed by dividing RHF by the latent heat of fusion (3.34e5 J kg^{-1}).

Text S3: Surface Energy Budget and Melt at KAN_M

In the lower ablation area at KAN_M, the initial pulse of the atmospheric river produces high melt rates, e.g. 61 mm d^{-1} at 1250 to 1350 m elevation. There, the atmospheric river more clearly peaks not only on 14th August but again on the 18th to a lesser extent when a thin ribbon of the AR is evident in ERA5 data (See Figure S1).

Text S4: Other AWS observations

NASA-SE

At NASA-SE (NSE), 5.2 mm of rain was recorded in two pulses: 13 August 12z-13 August 22z (ten hours) and from 14 August 16z-14 August 18z (two hours). During this time, 0.10 m snow deflation occurred. The deflation rate was highest when temperature was most elevated, suggesting sensible heat flux as the driver, not rainfall. Wind speeds do not correlate with deflation and were not peaking during rainfall (Figure S2b).

Swiss Camp and CP1

At Swiss Camp (SWC), rain totaled 11.2 mm, spanning 13 August 19z-15 August 13z, 42 hours (Figure S6a). At CP1 rain totaled 14.5 mm, spanning 13 August 20z-15 August 16z, 44 hours (Figure S6b). The 1.3x higher rainfall at CP1, 819 m higher in elevation, may be attributable to orographic intensification. At both sites, surface deflation is recorded.

Summit

The Summit GC-Net AWS recorded 0.15 m snowfall accumulation ten hours prior to the ~2 m air temperature (T_{air}) rising and staying above 0°C for seven hours. A distinct condensation gradient is observed at the time of T_{air} > 0°C. Wind speeds at the time of snowfall decreased and were elevated (~7 m s^{-1}). Little to no surface deflation occurred during the short-lived melting temperatures (Figure S5a) with reported rainfall.

References

Førland, E. J., Norske Meteorologiske Institutt., & Nordic Working Group on Precipitation (NWGP). (1996). Manual for operational correction of Nordic precipitation data. Oslo: Norwegian Meteorological Institute. Retrieved from https://www.worldcat.org/title/manual-for-operational-correction-of-nordic-precipitation-data/oclc/473734066

Goodison, B. E., Louie, P. Y. T., & Yang, D. (1998). Solid Precipitation Measurement Intercomparison (No. 872). WMO.

Li, X., & Kopp, R. (2019). Wetbulb calculation. Retrieved from https://github.com/smartlixx/WetBulb

Sevruk, B., Ondrás, M., & Chvíla, B. (2009). The WMO precipitation measurement intercomparisons. Atmospheric Research, 92(3), 376–380. https://doi.org/10.1016/j.atmosres.2009.01.016

Yang, D., Ishida, S., Goodison, B. E., & Gunther, T. (1999). Bias correction of daily precipitation measurements for Greenland. Journal of Geophysical Research: Atmospheres. https://doi.org/10.1029/1998jd200110

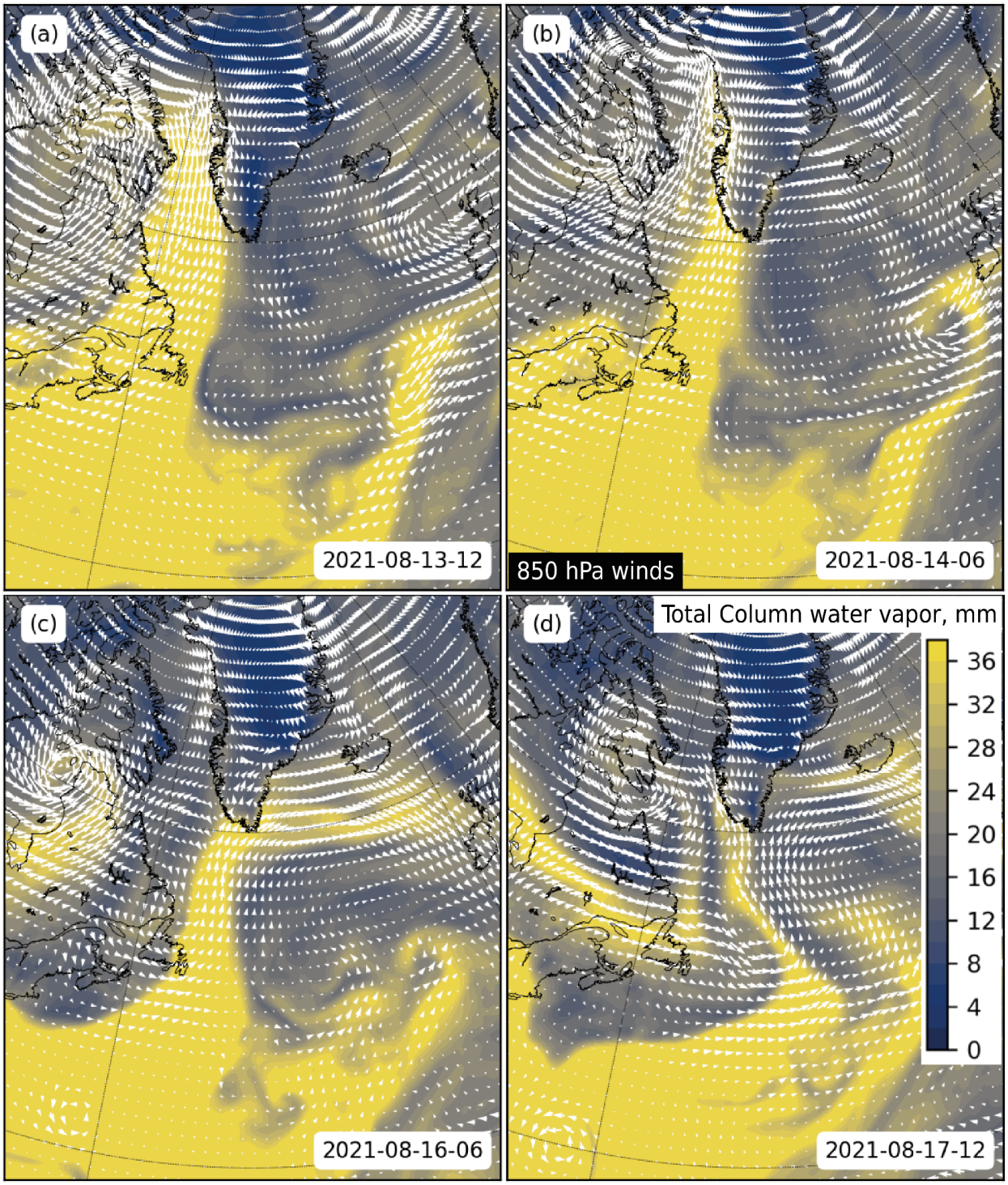

Figure S1. Select dates ERA5 total column water vapor and 850 hPa winds. The figure continues on the next page.

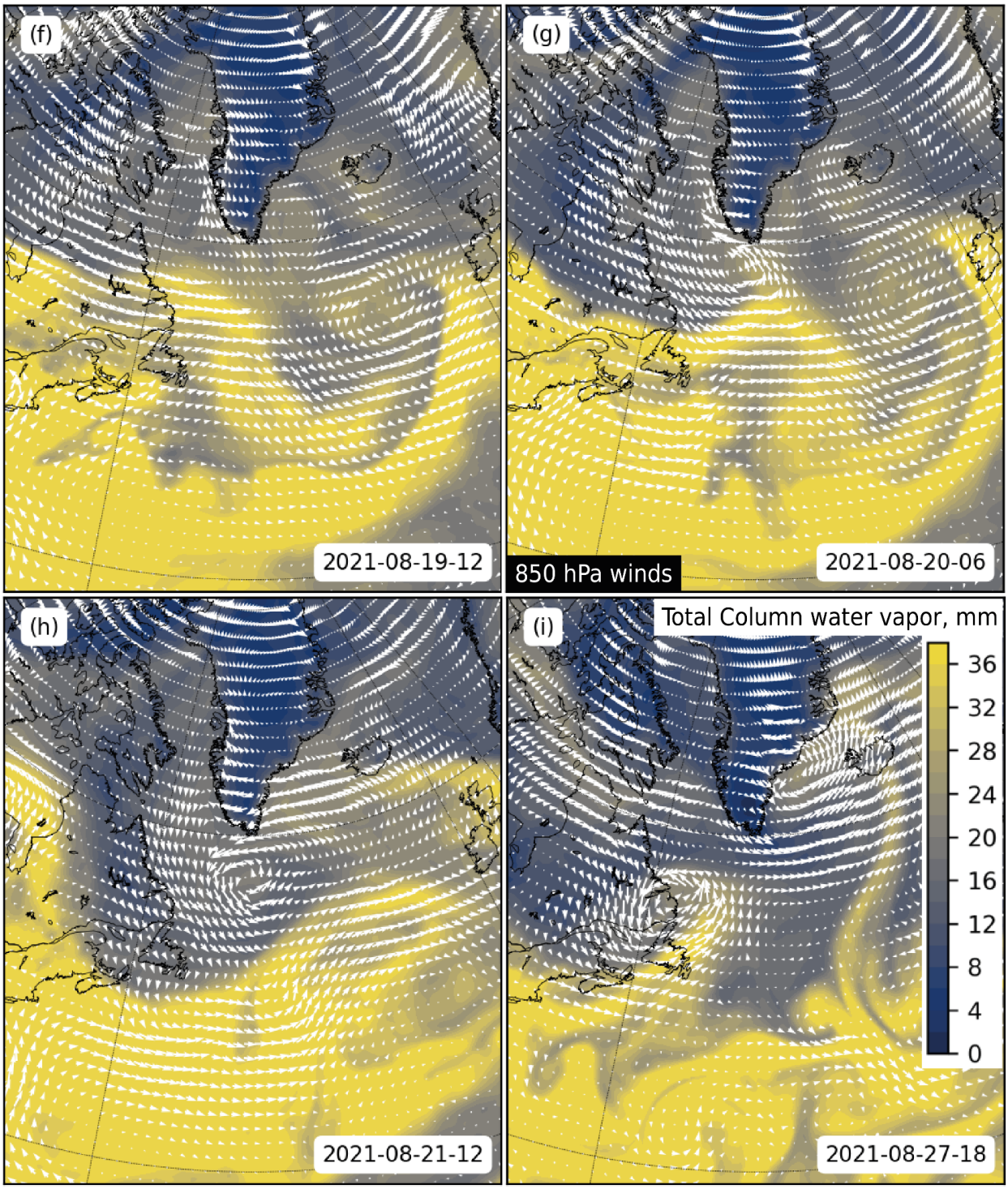

Figure S1-continued. Select dates ERA5 total column water vapor and 850 hPa winds.

The figure continues on the next page.

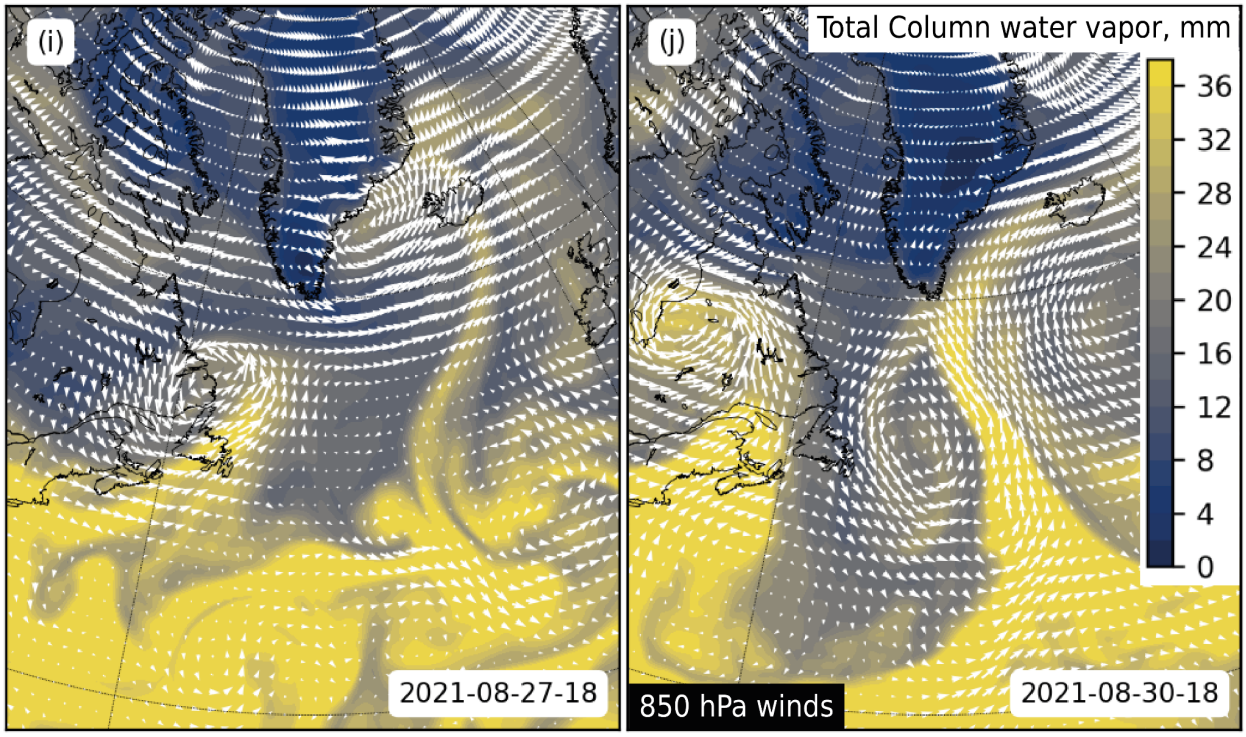

Figure S1-continued. Select dates ERA5 total column water vapor and 850 hPa winds.

Figure S2. *NUK_U PROMICE AWS with rain gauge (foreground) on 10 September, 2021_U and older PROMICE AWS version in background. Photo Jakob Jakpbsen.*

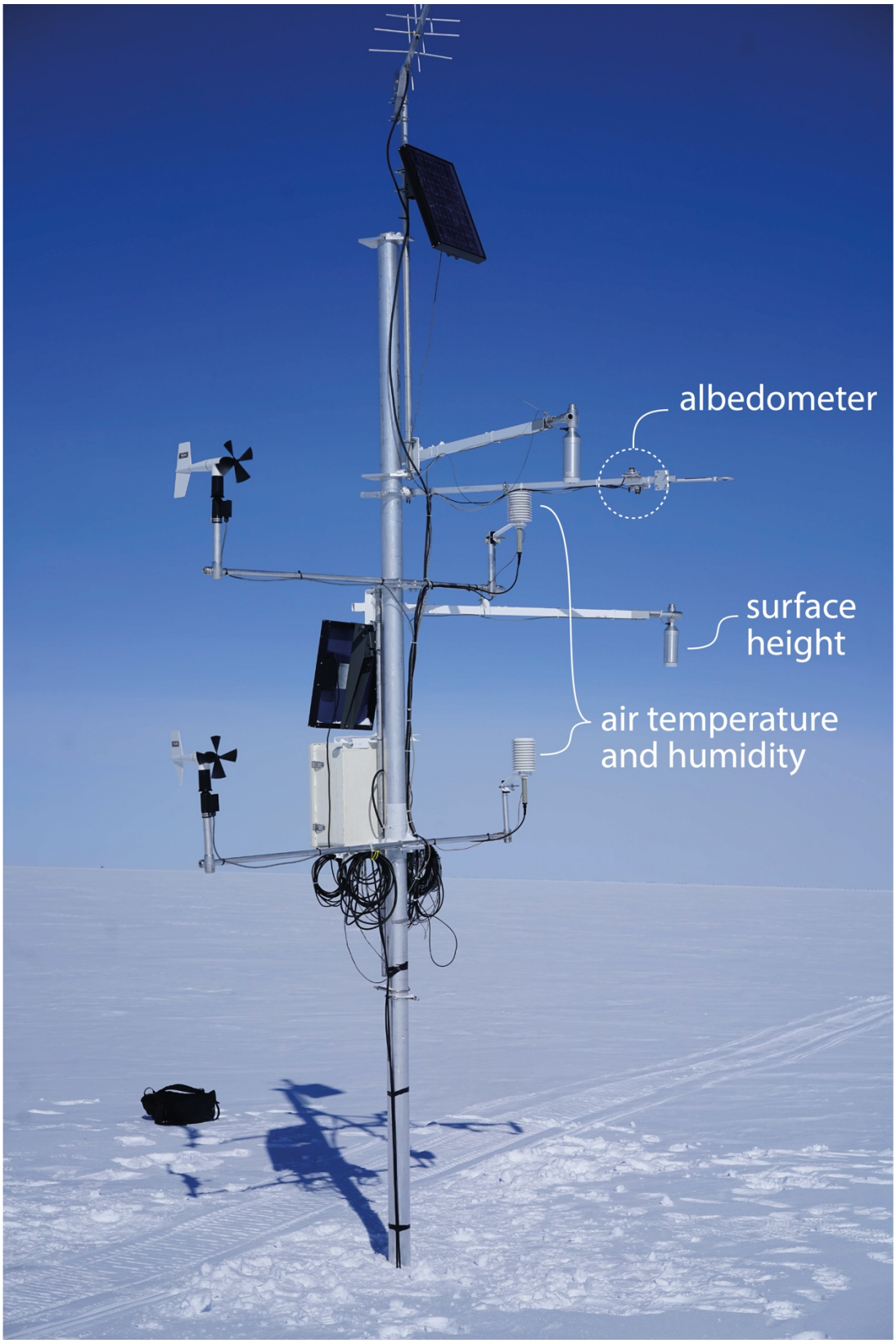

Figure S3. *GC-Net AWS at Summit. May 23, 2015 Photo K. Steffen*

Figure S4. Newly-installed GEUS GC-Net AWS at South Dome. June 21, 2021 Photo J. Box.

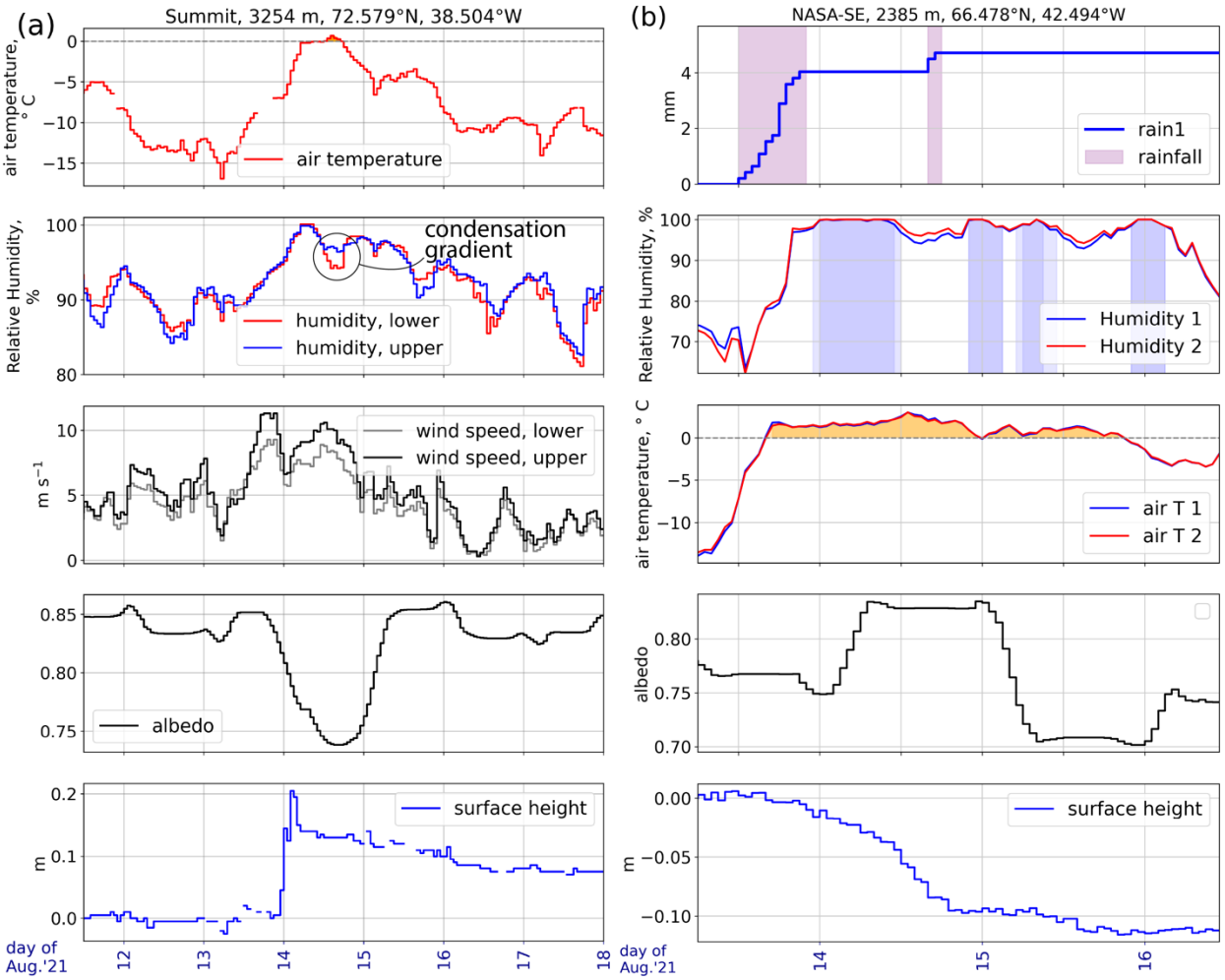

Figure S5. *GEUS GC-Net AWS records. Rain 2 at NASA-SE was malfunctioning.*

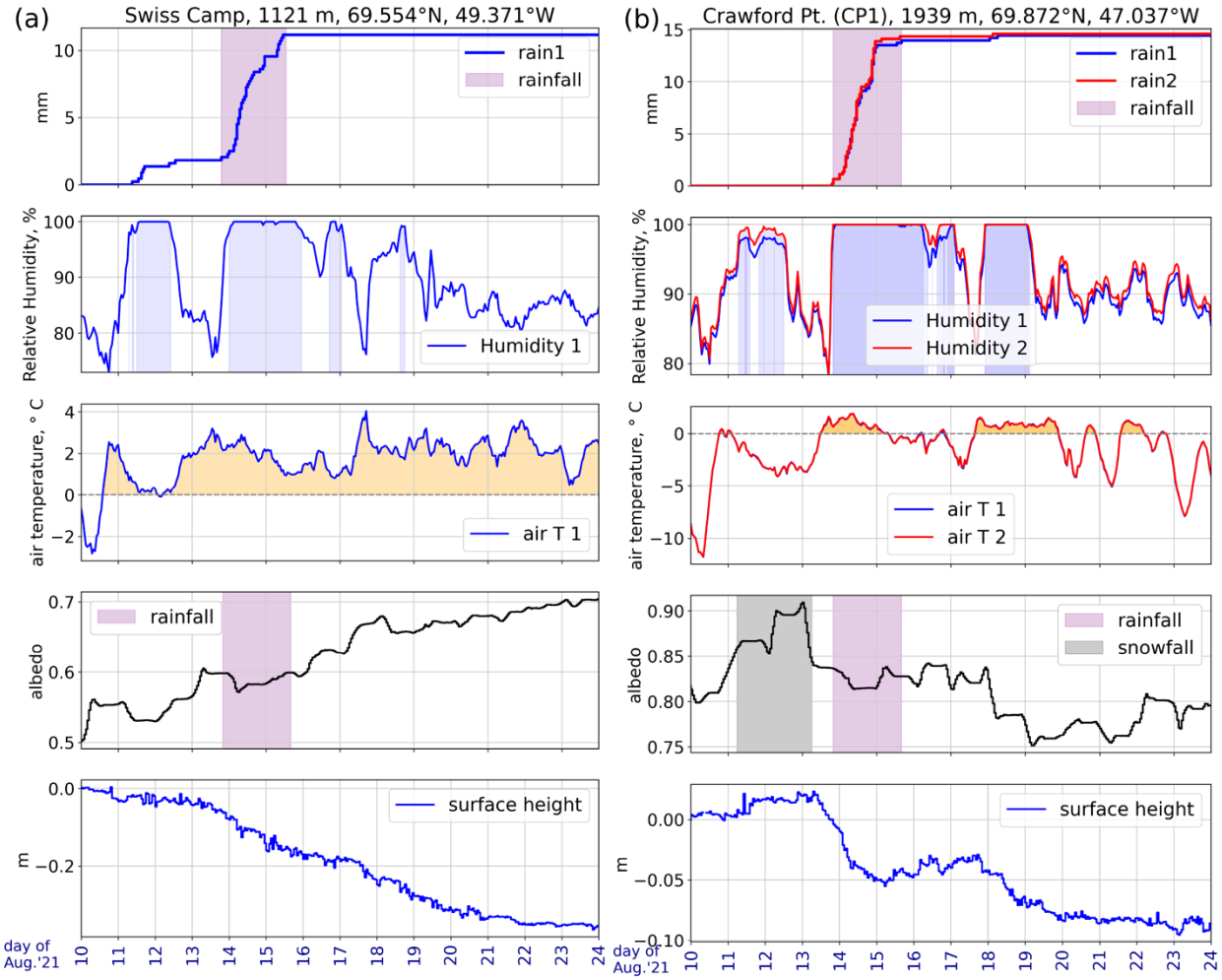

Figure S6. *GEUS GC-Net AWS records. Only one rainfall sensor was installed at Swiss Camp.*

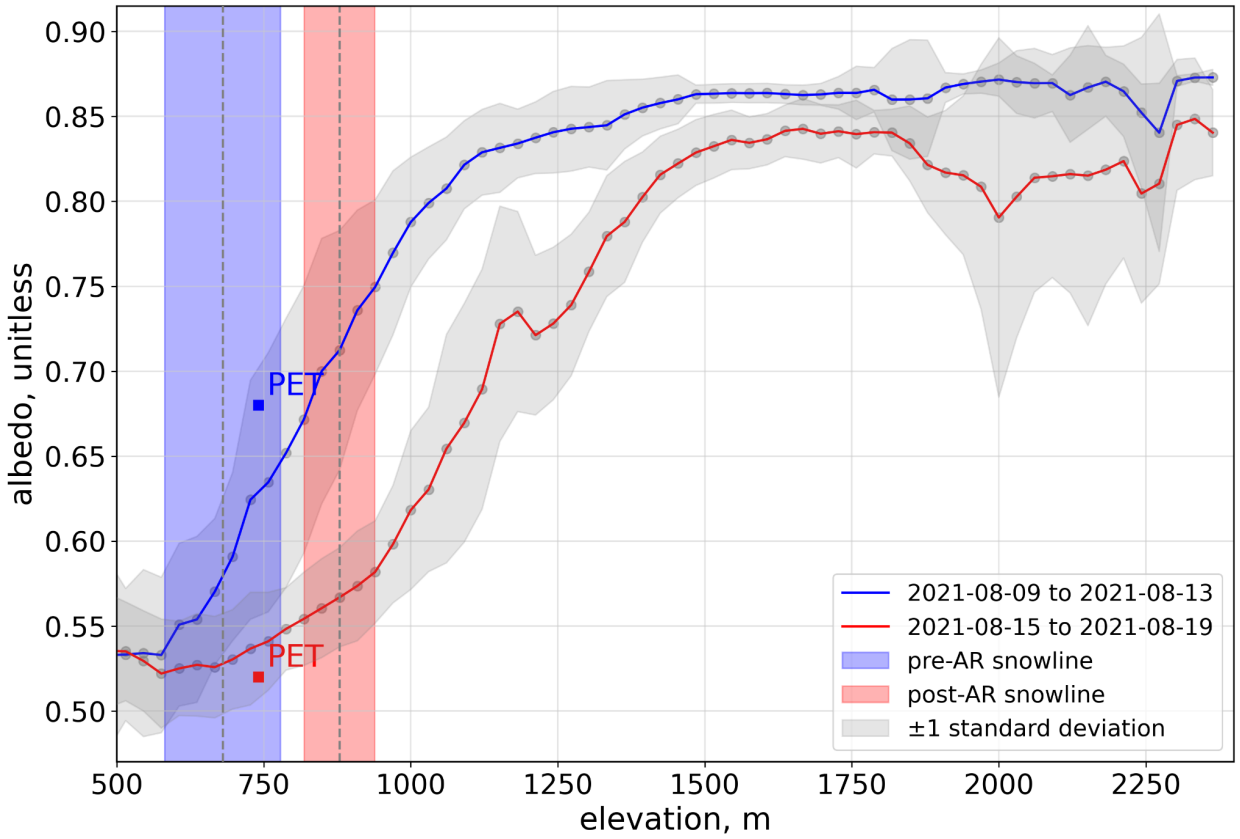

Figure S7. Averaged elevation profiles of albedo with field observations for the far northwestern Greenland ice sheet.

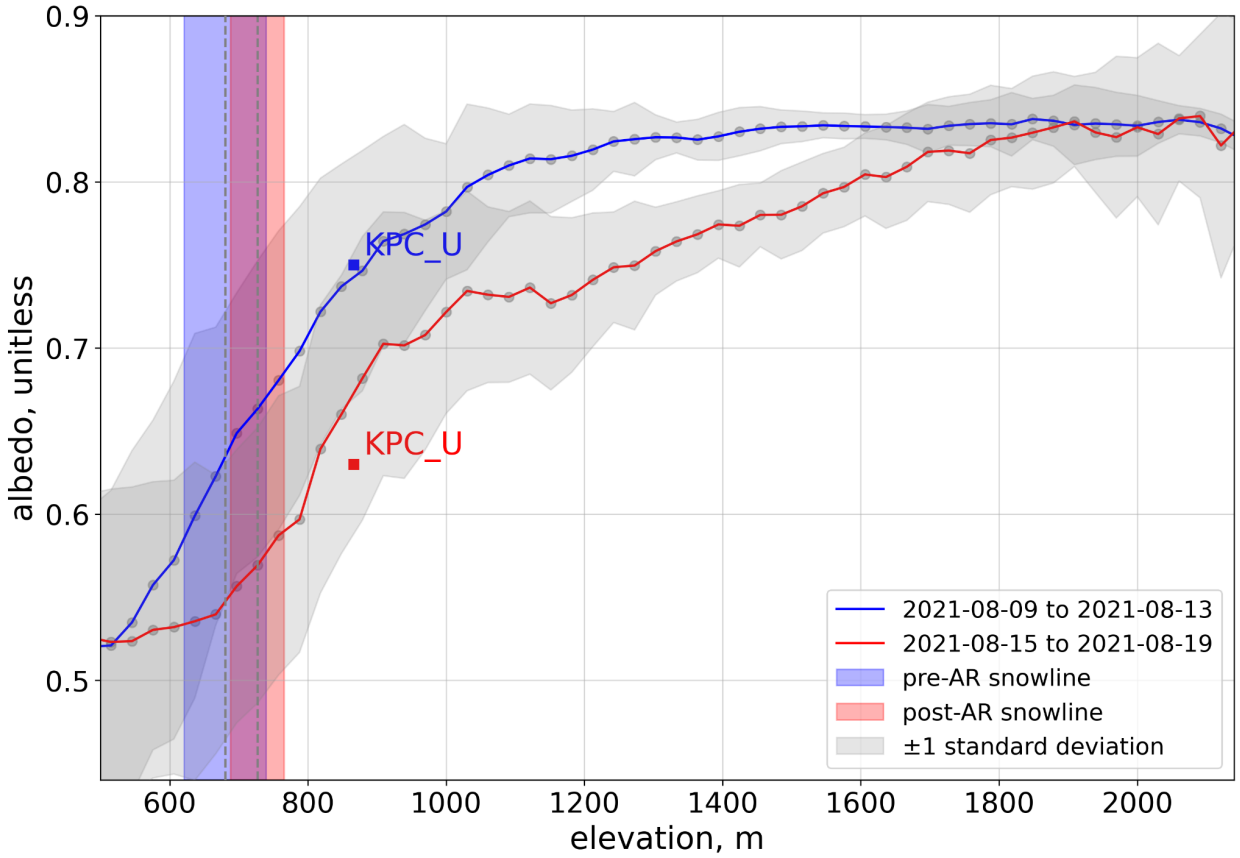

Figure S8. *Averaged elevation profiles of albedo with field observations for the northeastern Greenland ice sheet.*

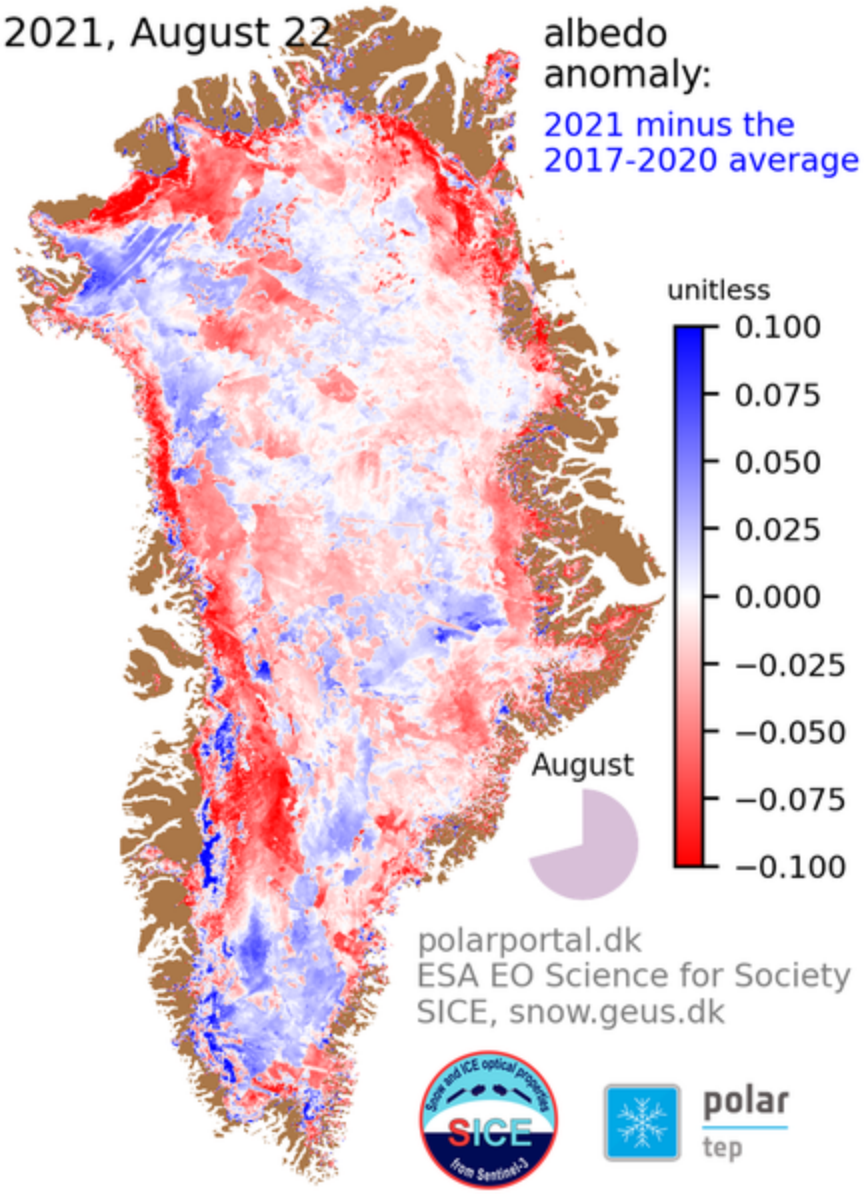

Figure S9. *Albedo anomaly map from polarportal.dk illustrates widespread dark anomaly in and above much of the ice sheet ablation area.*

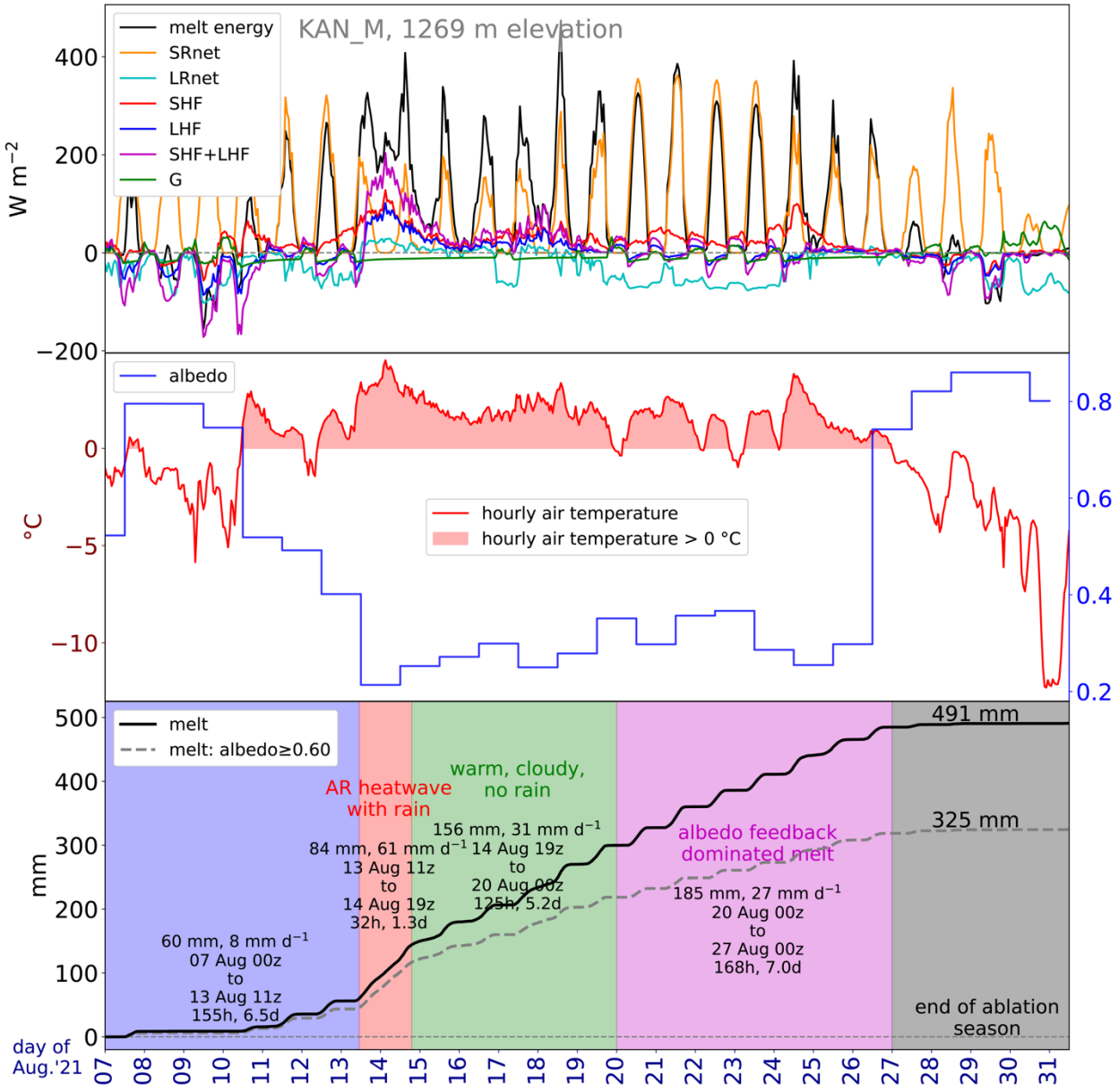

Figure S10. *surface energy budget and cumulative melting at the 1400 m elevation band in the Watson River catchment based on an elevation-based interpolation of KAN_L, M and U AWS observations and Sentinel-3 albedo data; calculations after* ***(van As et al., 2017)****.*

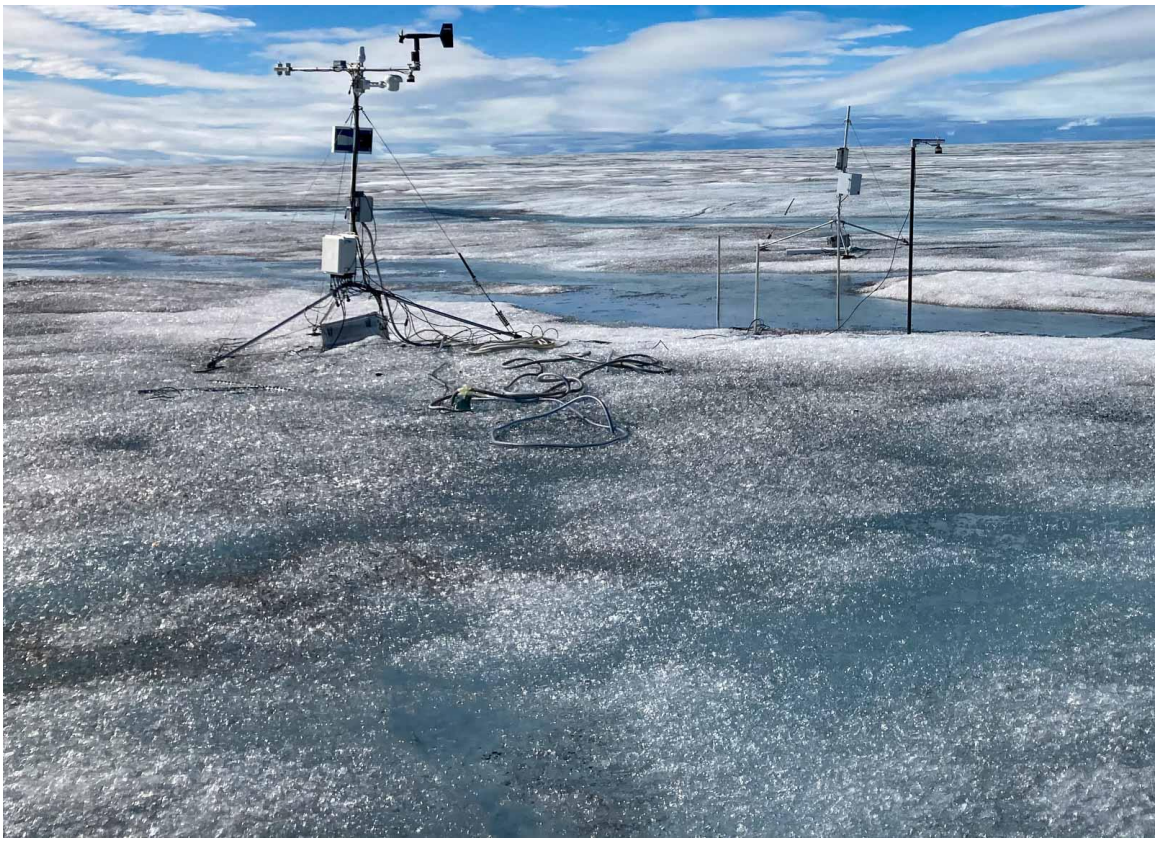

Figure S11. *water saturated ice surface at KAN_M, 18 August, 2019. Photo D. van As*

Figure S12. *difficulty walking in deep melting snow at KAN_U, 1843 m elevation, 18 Aug, 2021. Photo D. van As*

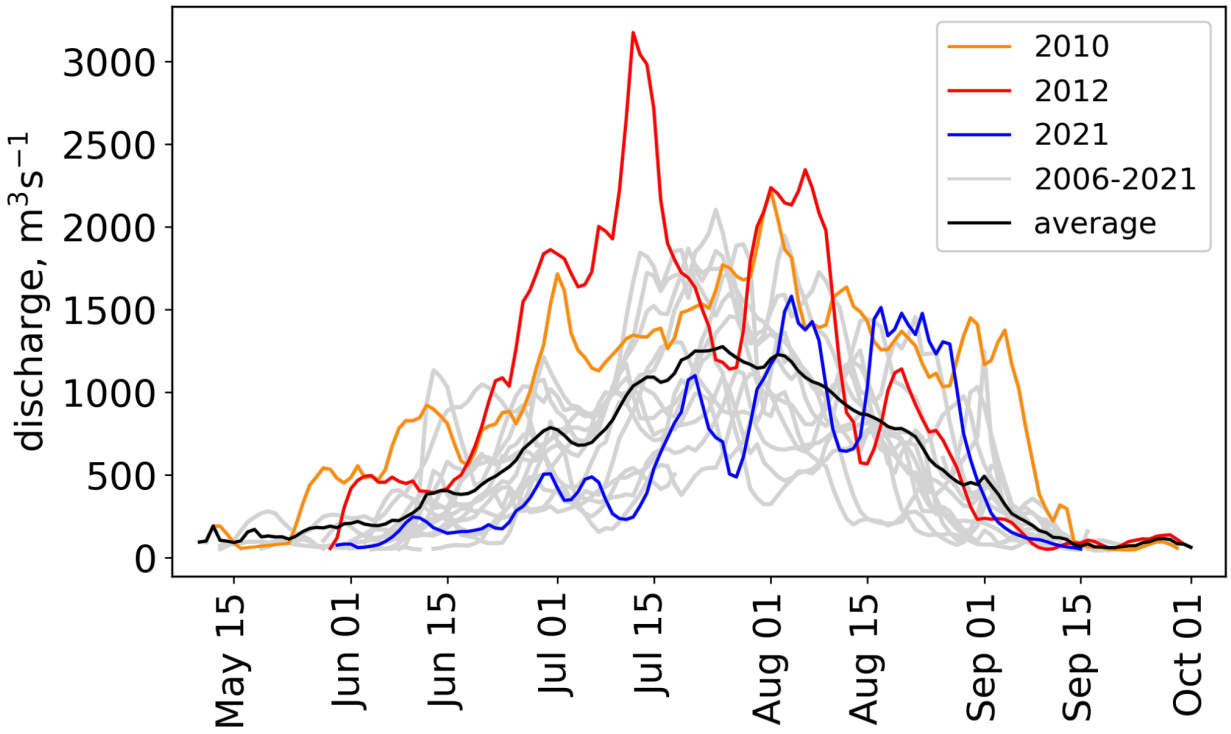

Figure S13. *Watson River discharge for the years 2006 to 2021. The high discharge years 2010 and 2012 are highlighted as well as 2021 and the 2006 to 2021 average.*